Spring 2020

Deposition and Characterization of Indium Nitride and Aluminum Nitride Thin Films by Reactive Sputtering

Sushma Swaraj Atluri
Old Dominion University, satlu001@odu.edu

DEPOSITION AND CHARACTERIZATION OF INDIUM NITRIDE AND ALUMINUM NITRIDE THIN FILMS BY REACTIVE SPUTTERING

by

Sushma Swaraj Atluri
B.Tech. May 2017, Jawaharlal Nehru Technological University, India

A Thesis Submitted to the Faculty of
Old Dominion University in Partial Fulfillment of the
Requirements for the Degree of

MASTER OF SCIENCE

ELECTRICAL AND COMPUTER ENGINEERING

OLD DOMINION UNIVERSITY
May 2020

Approved by:

Sylvain Marsillac (Director)

Christian Zemlin (Member)

Orlando Ayala (Member)

ABSTRACT

DEPOSITION AND CHARACTERIZATION OF INDIUM NITRIDE AND ALUMINUM NITRIDE THIN FILMS BY REACTIVE SPUTTERING

Sushma Swaraj Atluri
Old Dominion University, 2020
Director: Dr. Sylvain Marsillac

Intensive research has been carried out on III-V semiconductors for over a century due to their various applications in the field of Microelectronics, Optics, and Photonics. Among III-V materials, the III-nitrides, for example Aluminum Nitride, Indium Nitride, Gallium Nitride and their ternary alloys are known for their unique properties. All the III-Nitride Compounds are direct bandgap semiconductors with a bandgap ranging from 0.7 eV to 6.2 eV covering the entire visible region and extending to the UV region as well. Despite having many applications, fabricating good quality thin films without defects is quite a challenge. They are typically grown using a process called Molecular Beam Epitaxy (MBE) on substrates, such as sapphire or silicon carbide (SiC), but the process and materials are not very economical. The main aim of this thesis is to deposit high quality III-Nitrides thin films with the help of Reactive Magnetron Sputtering on various substrates. Various characterization techniques are used to analyze the samples and understand the effect of various deposition parameters on the quality of the films.

This thesis is dedicated to my parents, Nagabhushanam Atluri and Varalakshmi Venkata Padmavathi Atluri.

ACKNOWLEDGMENTS

First of all, I would like to express my deep and sincere gratitude to, Dr. Sylvain Marsillac for his continuous support and motivation which helped me achieve my endeavor. His dynamism, sincerity and vision have deeply inspired me. I would like to thank him for giving this opportunity to conduct research under his supervision. I would also like to thank him for his great sense of humor and patience during the discussions I had with him on research work and thesis preparation.

I would like to thank Dr. Orlando Ayala, Associate Professor of the Department of Engineering Technology, Old Dominion University and Dr. Christian Zemlin, Associate Professor of Electrical and Computer Engineering, Old Dominion University for their willingness to serve on my thesis committee besides their busy schedules.

I would like to offer special thanks to my colleagues and research members Ben Belfore, Hamza Kahoui, and Deewakar Poudel for their continuous support and helping me with the research.

I wish to extend a heartfelt thank you to my parents, Nagabhushanam Atluri and Varalakshmi Venkata Padmavathi Atluri for their love, encouragement, intense support and advice. Without your support I couldn't be this far. I love you for all the caring and your everlasting belief in me.

TABLE OF CONTENTS

LIST OF TABLES

LIST OF FIGURES

CHAPTER 1

INTRODUCTION

1.1 NEED FOR III-V SEMICONDUCTOR MATERIALS

Research on compound semiconductors has been going on for more than a century. Out of all the compound semiconductors, III-V materials have gained lot of attention over the years due to their applications in optics and photonics. III-V materials were primarily developed to produce different colors of LED's and to fabricate short-wavelength lasers, but nowadays these materials have applications in almost every field including solar cells, microelectronics, etc. The characteristics of these materials are comparable to the almighty silicon, which is the material of choice in every industry due to its impeccable properties, cost and abundance on earth's crust. III-V materials have several advantages over silicon. They have low effective masses, higher mobilities and can withstand high temperatures which makes them suitable for fabricating high-speed electronics. Silicon cannot be easily replaced by any other material but instead it can be combined with other materials to improve its existing capabilities [1]. Efforts are being made by several companies like IBM to integrate silicon with III-V materials [2] and soon we will have more efficient semiconductor devices with minimal cost of production.

1.2 III-NITRIDES MATERIALS AND PROPERTIES

The III-Nitride materials are formed due to bonding between Group III elements such as Boron, Indium, Gallium, and Aluminum with Nitrogen (group V). The key advantages of these materials are that they have direct bandgaps, which makes efficient absorbers and emitters of light. The optical band gap of these elements is ranging from 0.7 eV for Indium Nitride (InN), 3.4 eV for Gallium Nitride (GaN) and 6.2 eV for Aluminum Nitride (AlN). The various bandgap requirements can be met by forming Ternary alloy of these compounds like $Al_{1-x}In_xN$. By varying

the ratio of In and Al in the composites, the bandgap shifts from infrared to ultraviolet region which makes them suitable for solar cells, detectors, and various light-emitting devices such as light-emitting diodes (LED). III–V ternary and quaternary alloy systems are potentially of great importance to many high-speed electronic and optoelectronic devices, as they provide natural tuning of bandgap and widen the applications in the semiconductor industry.

The other advantages of these compounds include their remarkable electrical properties. The main reason for choosing III-nitrides over other higher bandgap materials is because they have a solid chemical bond which makes the material resilient to degradation. The chemical inertness of these materials has potential use in high power applications, radiation, and hostile environments. III-nitrides, especially GaN and AlN, have a high melting point so they can withstand high temperatures.

Aluminum nitride is the first nitride ever synthesized in 1907 [3]. III-nitrides can be available in three crystal structures: Wurtzite, zinc blende, and rock salt. Usually, III-nitride crystallizes in the Wurtzite structure since it is the most thermodynamically stable. Crystallization in other structures requires certain specific conditions. Wurtzite and zinc blende are identical; the only difference is the stacking sequence of tetrahedral atomic sheets. If there is a defect in growing the layer, we can observe the change in the structure from Wurtzite to zinc blende. The change in the stacking sequence mainly happens due to lattice mismatch of the substrate and film grown. Rock salt structure only forms under high pressure.

There are various challenges in growing nitrides, such as lack of suitable lattice-matched and thermally compatible substrates, inability to develop good quality crystals, and defects. The raw materials for fabricating the wafers are far more expensive and rarer. The most preferred substrates for epitaxial growth are Silicon carbide wafer and C-Sapphire. Extensive research is

going on for growing III-nitrides on Silicon substrates to make the process compatible with Silicon technology, and Silicon Substrates are economical when compared to sapphire and SiC.

1.3 THESIS OBJECTIVES AND ORGANIZATION

The aim of this thesis is to study fundamental properties and develop a process for depositing InN and AlN thin films using a non-epitaxial deposition technique and non-lattice matching substrates. III-Nitride materials have always been a challenge due to fabrication costs and quality of the films. Our effort is to fabricate these materials using reactive magnetron sputtering, which is relatively cost-effective and has quality comparable to that of traditional fabrication methods. Moreover, the effect of various deposition parameters on the Indium Nitride (InN) and Aluminum Nitride (AlN) thin films are studied and the results are compared with the references in order to optimize the deposition parameters.

In Chapter 2, an overview of III-nitrides synthesis and several characterization techniques (including XRD, Spectroscopic Ellipsometry, Hall effect) used are presented.

In Chapter 3, an overview of sputtering process and various sputtering parameters and operational particulars used for deposition of Nitride films are discussed.

In Chapter 4, a brief introduction about physical properties and applications of Aluminum Nitride films including the work done in this thesis with characterization results are presented.

In Chapter 5, a brief introduction about the physical properties and applications of Indium nitride films including the work done in this thesis with characterization results are presented.

Finally, Chapter 6 concludes the thesis and potential future work is presented.

CHAPTER 2

OVERVIEW OF III-NITRIDES SYNTHESIS AND CHARACTERIZATION

2.1 GROWTH OF GROUP III-NITRIDES

III-Nitrides are grown on substrates using either MBE (Molecular Beam Epitaxy) or MOCVD (Metal Organic Chemical Vapor Deposition) to obtain a single-crystal thin film. Single-crystal or monocrystalline materials are those who have a continuous lattice structure with no grain boundaries. Grain boundaries lead to defects, so a single crystal with no boundaries has no defects and has peculiar mechanical, electrical, and optical properties. Single crystals have applications in optics and electronics. To grow a single crystal, it requires high temperatures, sophisticated machinery, and controlled conditions. When it comes to the growth of III-Nitrides monocrystalline materials due to substrates lattice mismatch, there is much space for introducing defects. The lifetime of any optical devices such as LED depends on defect density: as the defect density increases, the lifetime of the device decreases. When going to high temperatures, there is a chance of forming nitrogen-deficient films and decomposition of the materials. When growing a single crystal of III-Nitrides materials, it not only has fabrication costs, but there can also be extra costs incurred with cutting and polishing. Preparing single-crystal films can be difficult and expensive when compared to polycrystalline counterparts.

Basically, there are two different ways for epitaxial growth. One of which is to grow bulk crystal and polish it, and the second approach is to grow the films on foreign substrates like C-sapphire, 6H-SiC, etc. [3]. Industrially, they use either Hydride vapor phase epitaxy (HVPE) or ammonothermal method to grow bulk crystals [4]. HVPE process involves the growth of III-Nitrides films by the reaction of Ammonia (NH_3) and the group III element, which is supplied by

the chlorides InCl, GaCl or AlCl. In the HVPE system, the chloride compounds are produced in situ by flowing HCl and reacting them with liquid Ga, In or Al elements at high temperatures.

These chlorides must be transported to the reactor zone. Nitrogen is supplied as Ammonia (NH_3) into the reactor zone. At high temperatures of the reacting zone, the Ammonia decomposes and reacts with the chlorides and form bulk crystal of III-Nitrides [5]. Using the HVPE method, the crystal quality of the film is affected. Ammonothermal method of growing bulk crystals has gained attention due to its ability to produce high crystal quality of GaN boules [4]. This method uses supercritical ammonia as a solvent to produce III-Nitrides crystals in an oxygen-free environment and the whole process takes place in a glove box [6].

The other way of growing good crystalline thick films of III-Nitrides on substrates is by using MBE or MOCVD. MBE is an epitaxial technique used to grow thin layers of single crystal III-Nitride material. This technique mainly uses “guns” to deposit material. Each element of the compound has a separate gun. The elements are heated up, evaporated and ejected from the gun towards the substrate. At the substrate, they react and form the desired compound. Advantages of using an MBE system is that the process takes place in a controlled and pure environment since MBE requires ultra-high vacuum free from contaminants. The growth of the layer is slow, which is an advantage and disadvantage too. Slow growth helps to develop defect-free and epitaxial films, but it is time-consuming and cannot be applied commercially. MBE of III-Nitrides have applications in high-speed electronics. [7].

MOCVD is the widely used technique for growing III-nitride single crystal thin film. MOCVD is commercially used to manufacture LEDs and to get the highest quality of III-nitride films. This technique does not require any vacuum. The ultra-pure gases are injected into the reactor and are deposited on to the substrate. Then these gases undergo surface reaction and form

the required elements. For MOCVD, the most often used substrate for III-Nitrides deposition is sapphire since it can withstand the high substrate temperatures. Also, sapphire has a lattice structure like that of III-Nitrides, especially for GaN. When growing films on a foreign substrate, the quality of the film gets better with thickness. Silicon (Si) substrates are widely being used as substrates due to their high quality, availability and are less expensive than sapphire. Using a Silicon substrate also makes the III-Nitrides devices compatible with silicon technology. The most used orientations of silicon substrates are Si (100) and Si (111).

There are several issues with the aforementioned approaches: the techniques of processing are extremely expensive and complex and even the raw materials can be toxic as well. Thanks to its relatively simple machinery, the technique of sputter deposition has gained attention in the last few years. MBE and MOCVD are primarily intended to develop an epitaxial film using a substrate with a similar lattice constant or by using a substrate with a different lattice constant but with the help of a buffer layer. For sputtering, however, the film is deposited and not grown. The key aim of using sputtering is to deposit a homogenous film on a large variety of substrates including amorphous or crystalline using low process temperatures. Sputtering deposition involves dislodging material from a target using ionized gas. The sputtered material will be deposited on the substrate. Deposition rate of sputtering depends on various parameters such as pressure and power. The higher the deposition rate, the lower will be the quality of the film and they tend to be amorphous or nanocrystalline. Nevertheless, using sputtering technique, III-nitrides films quality could be comparable to those fabricated with MBE and MOCVD techniques [8].

2.2 CHARACTERIZATION

2.21 X-RAY DIFFRACTION (XRD)

XRD is an instrument used to determine the crystal structure and to classify materials by means of their pattern of diffraction. XRD is fitted with an X-ray tube, a sample holder and a detector. The X-Ray tube is the primary source of X-Rays. The X-Ray tube consists of anode material such as copper and the wavelength of the X-rays generated is in the order of 1.54506 Å. The sample is placed in the instrument's center and illuminated by an X-Ray beam. The beam penetrates deep inside the material sample and a graph is traced from the signal diffracted from the sample to the detector that gives us crystallographic information. A MiniFlex II Benchtop X-ray Diffractometer (Rigaku) instrument was used in the thesis for XRD measurements.

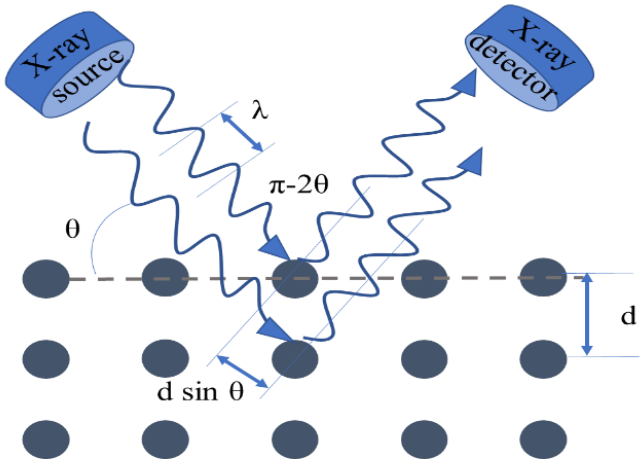

Fig. 2.1 Experimental setup for XRD measurements (based on 9).

Almost all the materials are made up of small crystals (except the amorphous ones of course). Each of these crystals is composed of regularly spaced atoms and each atom is composed of a nucleus surrounded by electrons. X-Rays are high energetic light rays with a specific wavelength. Since the wavelength of an X-Ray is similar to the distance between two atoms in a

crystal, a special interference effect, called diffraction, can be used to measure the distance between atomic planes. Interference occurs when the X-Rays interact with each other. If the X-Rays are in perfect alignment, the signal is amplified, and this is called constructive interference.

When the atomic planes are exposed to X-Rays, X-rays are scattered by the regularly spaced atoms. Strong amplification of the emitted signal occurs at very specific angles, where the scattered waves constructively interfere, this effect is called diffraction. The angle between the incident and diffracted beam is called 'theta' (2 theta precisely, see Figure 2.1). The relationship between the diffraction angle and the space between atomic planes can be determined using Bragg's law ($n\lambda=2d\sin\theta$), where n (an integer) is the "order" of reflection, λ is the wavelength of the X-ray, d is the spacing in between planes. The angle at which the peaks in the XRD scan occur is found with Bragg's Law. We can compare the obtained peak information by comparing the peak positions to the XRD database and retrieve the information about orientation, lattice constants and crystalline quality.

2.22 SPECTROSCOPIC ELLIPSOMETRY

Ellipsometry has several different areas of use and is a flexible thin film characterization technique. The key aspect of the technique is that it detects the change in polarization of the light which is reflected (or transmitted) from a thin-film sample. The exact change in the polarization depends on the film properties such as thickness, roughness, and complex refractive index. It measures two parameters Ψ and Δ, where Ψ, Δ gives the amplitude and phase difference respectively between the incident and reflected right. The polarization state of the light incident upon the sample may be decomposed into an s and a p component. Ellipsometry primarily measures the change in p and s components upon reflection. The p, s components are linear for the

incident light and when the light is reflected both these components undergo amplitude and phase change. The equation for change in polarization is written as [11]

$$\rho = \tan(\Psi)\, e^{i\Delta} \tag{2.0}$$

Ellipsometry can be used either for in-situ or ex-situ applications. It can measure optical constants of films with thickness less than 1 nm and up to 50 µm. We cannot directly measure thickness and several constants directly and in order to obtain the parameters, an optical model must be used. The surface of the sample should not be too rough for the use of ellipsometry. If the sample surface is too rough, the light scattering increases which reduces the intensity of the reflected light. The angle of incidence chosen for semiconductor thin films is in the order of 60-80° [12]. This technique can also be employed for films of unknown materials, since it is a model-based approach. We can also derive the optical properties of the unknown materials and it is only possible if the structure of the film is not complex i.e., single layer with a known substrate.

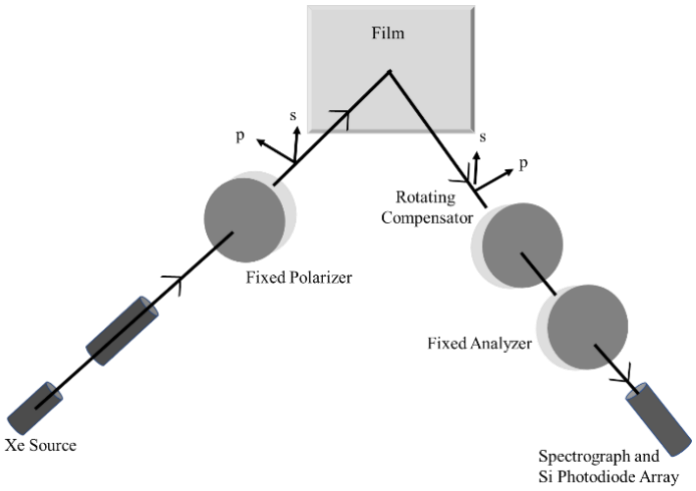

Fig. 2.2 Configuration of Ellipsometry (based on 12).

The key components of the experimental setup of the ellipsometry system are: (1) light source, (2) polarizer, (3) compensator, (4) analyzer, and (5) detector. There are also several configurations of ellipsometry which include rotating analyzer (RAE), rotating polarizer (RPE), rotating compensator (RCE), and phase modulation (PME) [9]. The light source can be a laser, xenon arc lamp or quartz tungsten halogen lamp, which produces an electromagnetic radiation in the form of light. The light generated by the light source is unpolarized and it passed through a polarizer. The polarizer is used to change the unpolarized light to linearly polarized, with p and s planes. When the sample is illuminated with the polarized light, it reflects from the surface and become elliptically polarized which is then passed through an analyzer, given orientation relative to the electric field. Finally, it reaches the detector which converts the light signal to electronic signal. This information is compared to the optical model and properties of the films are retrieved.

2.23 HALL EFFECT

Hall effect measurement is an electrical characterization technique that is primarily used to measure the resistivity, carrier concentration and carrier type of semiconductor material. Hall effect measurements are based on Lorentz force law. A particle of charge q moving with a velocity v in an electric field E and a magnetic field B experiences a force of

$$F = q[E + (v \times B)] \tag{2.1}$$

Hall effect is the production of a voltage difference across the conductor, transverse to both electrical current in the conductor and to an applied magnetic field perpendicular to the current. This induced voltage due to the applied magnetic field is known as 'Hall Voltage'. In order to measure the carrier concentrations, carrier type, and mobility, a series of resistance measurements are performed. These measurements are useful in classifying the material as a conductor or an insulator. This measurement requires a voltmeter to measure the potential difference induced,

current source to able to supply current in the range of mA to pA, Ammeter to measure the provided current, and a magnet with a strong magnetic field.

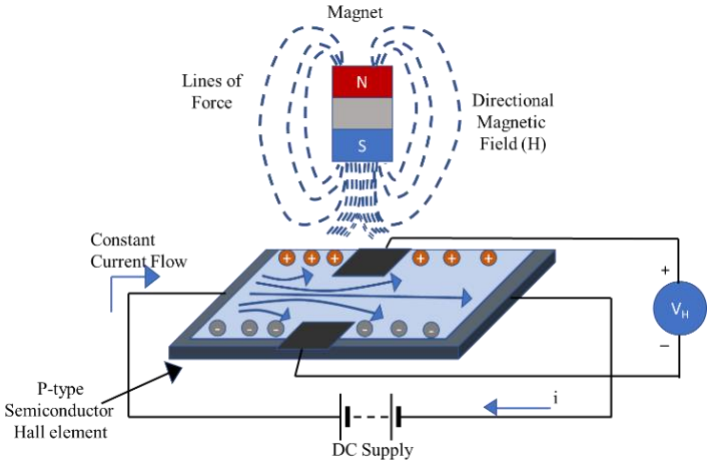

Fig 2.3 Hall effect measurement setup (based on 13)

As illustrated in Fig 2.3, a semiconductor wafer is used as Hall element, in which the majority carriers are holes. A constant current is flowing through the bar with applied DC voltage and a magnetic field is applied perpendicular to the flow of current. Since the holes are travelling through the magnetic field, they experience upwards Lorentz force and accumulate at the top of the bar. Due to the lack of holes on the bottom side of the bar, it will have a negative charge. This leads to a potential difference, which is called Hall voltage [14]. Two types of sample geometries are used to measure the hall effect: (1) Van der Pauw, and (2) Hall bar. Hall bar measurement type has six contacts and it is difficult to fabricate the geometry. Most used is Van der Pauw geometry, that offers four points of contact and can be made by cleaving the sample in the form of a square. Contacts are made on the corners of the square using Indium paste and the quality of the measurement is comparable to Hall bar. If the hall voltage measured is negative, then the material

is n-type and is positive for p-type. Once the hall voltage is obtained, mobility, sheet density and resistance can be calculated.

CHAPTER 3

OVERVIEW OF SPUTTERING PROCESS

3.1 INTRODUCTION TO SPUTTERING

Different techniques exist for depositing thin material films on various substrates. The thickness of these films can range from several nanometers to several micrometers. The substrates can be a semiconductor wafer or even a semiconductor device like a solar cell. Sputtering is one of the commonly used high vacuum physical vapor deposition techniques because it offers high-quality film and complete flexibility. The sputtering technique is based on ion bombardment of a target material which is also referred to as the source material. A gaseous plasma is created and the ions from the gaseous plasma are accelerated towards the source material and this results in the ejection of source material in the form of atoms or molecules. The ejected particles will travel along a straight path and get deposited on the substrate forming a thin layer of source material. Generally, a gas such as Argon is used as ionization gas due to its inertness and high sputter yield. Another reason to use argon is because the process is mainly used to deposit pure materials, but it can also be extended to deposition of compounds by using reactive gases such as oxygen or nitrogen and this process is called reactive sputtering.

The gas is ionized by free electrons from the negatively charged cathode and is accelerated away from it. These free electrons knock off an electron from the neutral gas atom outer shell, making the gas atoms ionized and positively charged. The positive ions are accelerated to the negatively charged source material due to coulombic attraction and bombard the surface of the target. The bombarding results in atoms being ejected and get deposited on a substrate. During the ejection process, not only atoms but electrons are also knocked off the target which will help in the formation of ions. As the gas ions are unstable, some of the free electrons find their way back

to the outer shell of the ions. These free electrons have some energy and they must return to the ground state by emitting the energy in the form of a photon. Photons are nothing but light particles and that is the reason we observe a glowing plasma.

3.11 GENERATION OF ENERGETIC IONS

Initiating the sputtering can be done in two ways. One way is to use an ion gun that is focused on the target and the gun is supplied with the gas. By applying suitable voltage, ions are generated. This process of generating ions is called ion beam sputtering and it is mostly used for analytical techniques such as SIMS. Another way of generating ions is by creating a plasma and the process of creating a plasma was discussed in the above section. When a high voltage difference is applied between cathode and anode, a glow discharge is observed.

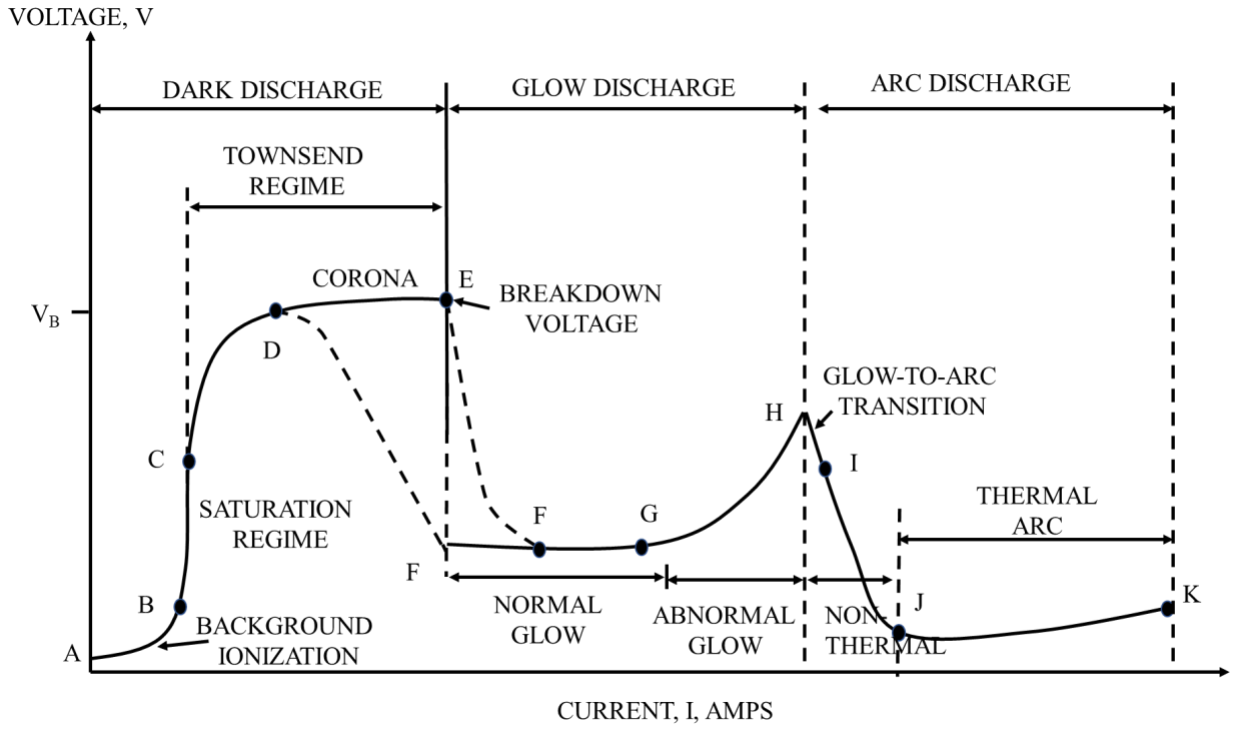

Fig 3.1 Regions of glow discharge (based on 16).

The main characteristics of the discharge depend on the positioning of the electrodes, vacuum vessel, types of gases used and electrode material. In a normal sputtering system, a vacuum is created using a turbo and roughing pump and it is pumped to a base pressure of 10^{-7}torr. A cathode and an anode are placed opposite to each other. There are three regions of glow discharge namely, 1) dark discharge, 2) glow discharge, and 3) arc discharge which can be understood by observing the I-V characteristics in figure 3.1 [15]. The first region known as the dark discharge is in between the points (A-E) and it got its name because the discharge occurring in this region is invisible except for corona and break down region. The discharge occurring in between A and B, due to background ionization, move towards the electrodes and produces a weak electrical current. The saturation regime occurs between B and C, where an increase in the applied voltages increases the current until B. As the applied voltage increases, the number of ions and electrons reaching the electrode will increase and then becomes saturated until C, where the current remains constant with the increase of voltage.

As the voltage is further increased, a sharp rise in current can be noticed in region C-E which means more ions are produced. The current increase observed is due to the impact ionization of atoms by the electrons. Hence rapid increase in the electron and ion production will increase the current. The C-E region is also known as the Townsend discharge region.

Corona discharge occurs between the D-E region. When the corona current is high, we can observe the glow of the discharge and if the current is low, the entire region is dark. Eventually, a breakdown is caused by the introduction of secondary electrons released from the cathode by ion and photon impacts in sufficiently strong electrical fields. At the breakdown point E the current might suddenly increase due to the high potential but it is limited by the resistance of the power supply connected to the plates. If the internal resistance is too low, then the gas will break down

at the indicated voltage and move into the usual discharge regime F-G The region F-G is in the glow discharge region and contrast with the dark region, so one can observe the plasma glow during sputtering.

3.1.2 SPUTTERING YIELD

The sputtering yield, Y, is defined as the average number of particles removed from a target per incident particle. Yield depends on the target material, bombarding ion species and their energy and angle of incidence. According to Sigmund's theory, the sputter yield at threshold ion energy is given by:

$$Y = \frac{3}{4\pi^2}\alpha\frac{4M_1M_2}{(M_1+M_2)^2}\frac{E}{U_s} \tag{3.0}$$

Where E is the Kinetic energy of the ion, M_1 and M_2 are the masses of bombarding ion and the target, U_s is the bonding energy of the target material, α is the angle of incidence of the ion. High energy ions sputter atoms by transferring energy greater than the binding energy of the target surface atoms and knocking them out. The ion energy usually will be higher than the binding energy and that is responsible for inelastic collisions, causing secondary electrons. These secondary electrons will help in sustaining the plasma. The higher the binding energy the higher will be the yield, but after a certain point, the yield starts decreasing because the ions start impinging into the target material which causes ion implantation instead of sputtering.

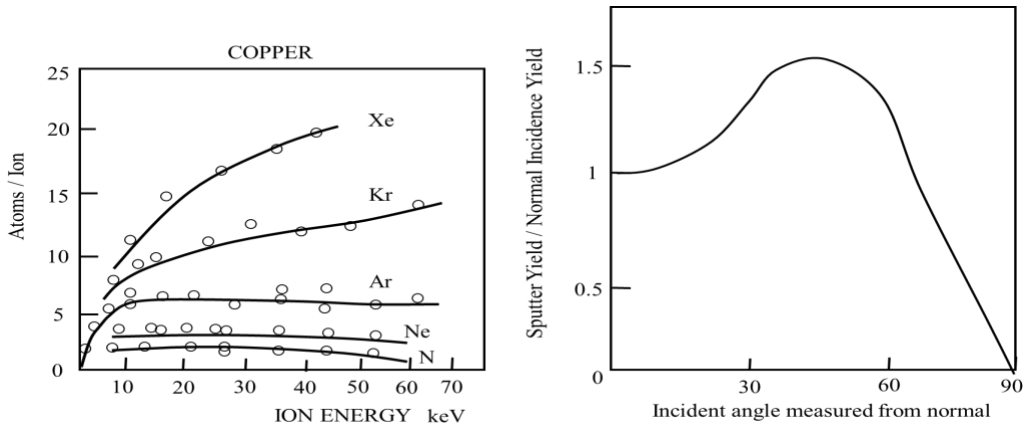

Fig 3.2 yield of gas ions vs ion energy and angle of incidence on copper (based on 17,18)

Maximum energy transfer occurs when the mass of target and ion are equal. For this reason, we generally use noble gases like Argon. From the above Figure 3.2, we can observe that the sputter yield increases with the mass of the ions also when comparing the sputter yield of Nitrogen to Xenon at 50 keV ion energy, xenon has a high sputtering yield because of its mass which is approximately 10 times higher than Nitrogen. Also, the sputter yield tends to increase with the increase in the obliqueness θ and the maximum sputter yield was observed at around 60º angle of incidence. At a higher angle of incidence, due to surface implantation, the yield decreased drastically.

3.2 REACTIVE SPUTTERING

Sputtering usually takes place using an inert gas such as Argon. Not only for depositing pure metals targets but it can also be used to deposit metal alloys, which helps to deposit complex coatings. Sputtering using inert gas is known for simplicity in the process, as it requires basic process controls. By adding a reactive gas to the sputtering, we can form a compound of the target and gas molecules. Using reactive gas compounds like nitrides, oxides, etc. are formed. To

distinguish this process from inert gas sputtering, it is called reactive sputtering. The process of reactive sputtering looks like normal sputtering, but it can be quite complicated. Introducing reactive gas not only changes the yield and deposition rate but also affects the composition of the target.

The figure 3.3 shows the basic reactive sputtering system. The system consists of a chamber, gas inlet, target, vacuum pump, and a power supply either DC or RF. Sputtering can be carried out either using sputter up or sputter down configuration. The one shown below is a sputter down configuration with target on the top and substrate at the bottom. The gases are introduced in the chamber using the inlet. The pump is used to maintain high vacuum in the chamber, and it will be constantly pumping throughout the deposition. The gases are fed to the system for ionization and they are transformed into the plasma state. With enough potential applied to the target, the gas ions are accelerated towards the target and collisions happen on the target surface.

The ejected ions react with gas molecules and form a compound, which is deposited on the substrate. The distribution of the reactive gas inside the chamber is an important consideration. The reactive gas is chemically just used to form the desired compound, whereas the inert gas atoms can be reused in plasma. To produce a consistently reacted film, certain physical means to uniformly inject this gas through the whole plasma around the cathode often need to be incorporated. The most effective way of introducing the gas is by using a gas ring around the target. This gas ring has small perforations to allow the gas into the plasma at regular intervals of time. Like inert gas, the reactive gas will also ionize, gets accelerated to the target and sputter the material from the target. Some users will only use non-inert gas as process gas, but the sputter rate will be affected and there is a chance of poisoning the target.

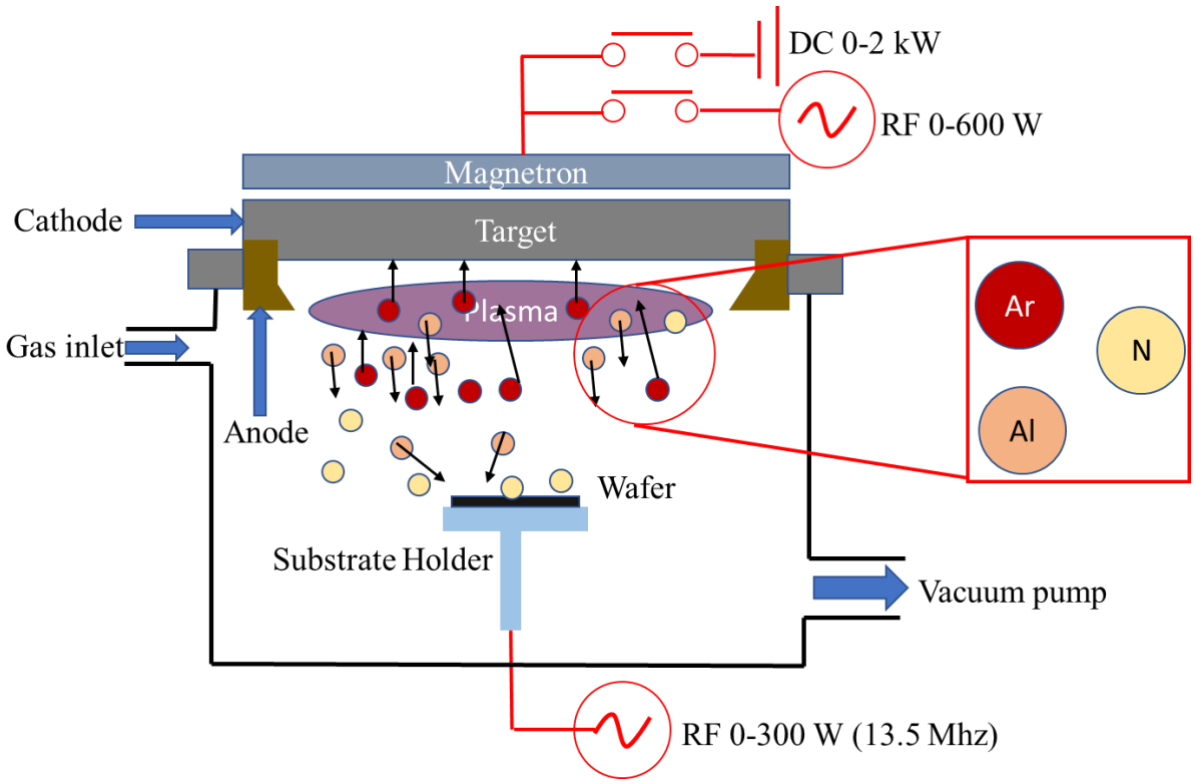

Fig 3.3 Reactive sputtering system (based on 19)

3.2.1 HYSTERESIS EFFECT IN REACTIVE SPUTTERING

The reactive sputtering can be operated in three different mode:1.) metallic mode, 2.) transition mode and 3.) reactive mode. These modes are very susceptible to the reactive gas supply. These processes must be controlled very well for the stoichiometric deposition of the thin film. In the metallic mode, the deposition rate of the metal target will be high, and the composition of the thin films will not be stoichiometric. If a high amount of gas is supplied to the target, then stoichiometry will be maintained but it will cause poisoning of the target which will, in turn, affect the deposition rate. The transition from one mode to another often leads to the effect of hysteresis depending on the reactivity between the target and reactive gas and on the various process parameters.

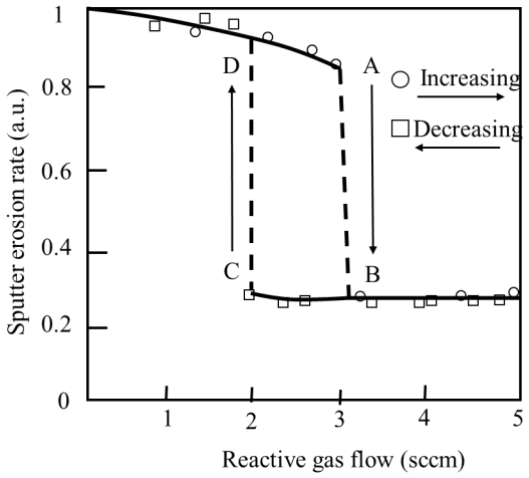

Fig 3.4 Effect of reactive gas flow on rate of sputtering (based on 20)

From the above figure 3.4, we can observe the drastic changes in sputtering rate with change of gas flow rate. The increase in reactive gas flows slightly beyond the point A in the figure will lead to an abrupt transition in the rate down to point B. Reducing the reactive gas volume to the point C, the rate is suddenly increased to point D. Due to this hysteresis loop it will be extremely difficult to control the process parameters of reactive sputtering

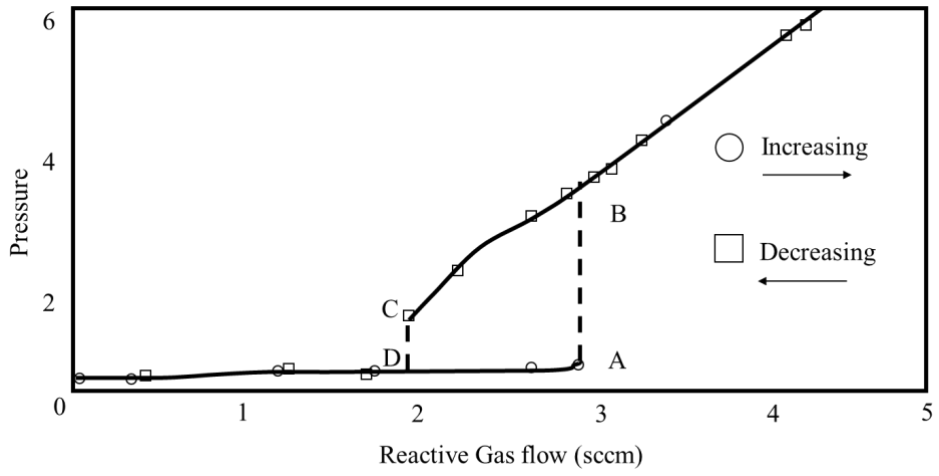

Fig 3.5 Effect of reactive gas flow on partial pressure of the gas (based on 20).

The process parameters of the above figure are considered in figure 3.5. The gas flow is increased to point A, which is the starting stage of the sputtering process. At point A, the target is completely metallic, and the partial pressure of the gas is low. At point B, it can be observed that the partial pressure of the gas is increased which is due to the transition from metallic mode to reactive mode. Even though the flow rate of gas is decreased to point C, the partial pressure of the gas remains significantly high.

Let us consider the case of Aluminum nitride (AlN) in the presence of Argon and Nitrogen gases as sputtering species. It is known that the sputtering yield of the Al target is higher than that of AlN. When only Argon is introduced into the chamber, from the above figures 3.4 and 3.5 the rate of the sputtering is high. When the nitrogen is slowly introduced into the chamber, the sputter rate and partial pressure are significantly affected because most of the gas is consumed to form the compound at the substrate. AlN can also be formed on the target but due to the high sputter rate of argon, the surface of the target will be cleaned of any compound formed at position A. Conditions are created in that position which forces the partial pressure to dramatically increase to position B.

This new partial nitrogen pressure is sufficiently high to form AlN on the entire target surface. The target is said to be in the poisoned mode from position B. Due to the poisoning of the target, the deposition rate will be defined by the low sputtering value of AlN formed on the target surface. The excess nitrogen in the chamber which remains after formation of AlN will cause an increase in the partial pressure. As less Al is eroded after transition A-B, excess nitrogen will add up to the high partial pressure. Therefore, during nitrogen flow decreases the nitrogen partial

pressure will be higher. This is valid until the partial nitrogen pressure is not sufficiently large to fully form AlN on the Target. After point C, the target will be again transitioning to metallic mode down to point D. From point D, sputter yield is only dependent on Al [20].

3.3 POWER FOR REACTIVE SPUTTERING

The disadvantage of using sputtering is that when the gas pressure is lowered the ionization efficiency is also decreased because the gas ions are ionized far away from the target and get lost in the chamber walls. To solve this problem, most of the sputtering targets are employed with a magnetron source. The advantages of using a magnetron sputtering are high deposition rate, ease of sputtering any compound, alloy, and extremely high adhesion of films. Figure 3.6 shows the schematic of the magnetron source. The operation of a magnetron source is essentially based on the fact that in a localized region close to the cathode the primary and secondary electrons are trapped in an endless track. This greatly enhances their chances of an ionizing collision with a gas atom and therefore increases the efficiency of ionization. Magnetron source can be powered using RF or DC power supply. While sputtering is a cost-effective solution for many types of metal coating, its main restriction consists of using non conducting targets or an insulating film that can be formed when doing reactive sputtering like AlN, which will cause arcing near the target material due to charge build-up. Ultimately, that will affect the quality of the films.

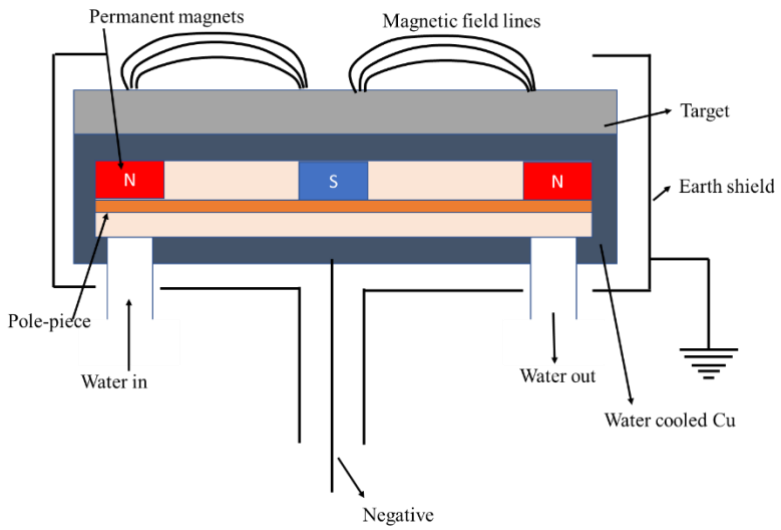

Fig 3.6 schematic of magnetron source (based on 21).

To overcome the problem of sputtering insulating materials, RF power supply is being used. Radio frequency magnetron sputtering is the technique in which an alternating electric field is applied to the target to clean the charge buildup. The magnet behind the cathode is used to trap the electrons near the target material and it will not allow them to bombard the target increasing the deposition rate. Overtime positive ions start building up on the target making it positively charged because of this instead of attracting, the target starts repelling the positive ions which will cause a complete cessation of sputtering. When a positive potential is applied to the target, all the charge buildup will be cleaned of the target surface. During the negative cycle, as usual sputtering process, ion bombardment with the target continues. For reactive sputtering it is always better to use RF magnetron sputtering because there is a chance of poisoning the target. The poisoned layer can act as an insulator and, by using RF magnetron sputtering, the surface of the target material can be cleaned of a charge buildup with each cycle.

CHAPTER 4

EFFECT OF SPUTTERING PROCESS PARAMETERS ON ALUMINUM NITRIDE THIN FILMS GROWTH

4.1 PROPERTIES OF ALUMINUM NITRIDE

Aluminum Nitride (AlN) is a member of group III- Nitrides and it is a wide direct bandgap material with bandgap around 6.2 eV. It has a potential application in optoelectronics operating at deep ultraviolet frequencies. The lattice constants range from 3.110 Å to 3.113 Å for the a-axis, and from 4.978 Å to 4.982 Å for the c-axis [19]. The index of refraction in the visible is in the range of 2.1-2.2 for single crystals and 1.8-1.9 for amorphous films. Aluminum Nitride (AlN) is a unique ceramic material that combines high thermal conductivity with high electrical resistivity [22]. There are only few other semiconductors like beryllium oxide (BeO) and boron nitride (BN) with a high thermal conductivity. Beryllium oxide is replaced with Aluminum nitride in semiconductor because of its toxicity. Aluminum nitride remains stable in inert atmosphere at high temperatures and starts melting at 2000ºC.

The advantages of aluminum nitride are as follows [22]:

- Its high thermal conductivity, theoretically 285 W$m^{-1}K^{-1}$
- very high electrical resistivity
- a high dielectric constant
- a thermal expansion coefficient closer to that of silicon than alumina
- An excellent resistance to corrosion

Aluminum nitride has two potential crystal structures: hexagonal wurtzite and cubic sphalerite. Hexagonal wurtzite crystal is the most stable structure, whereas cubic sphalerite is a metastable structure and can be stable at higher pressures.

Applications of aluminum nitride

Aluminum nitride is one of the few materials that provides a high thermal conductivity and electrical insulation. This makes AlN extremely useful for high-performance electronic applications in thermal sinks and heat spreaders.

Aluminum nitride LED produce 210 nm radiation. It is used to eliminate toxins from the environment, and it is an eco-friendly alternative to chlorine to treat drinking water.

Also, Aluminum nitrides thin films can be used in piezoelectric applications such as energy harvesters [19].

Sputter parameters for the aluminum nitrides films

We used an AJA Orion 8 sputtering system with a KDC-40 ion beam controller and a multi target sputtering system. The target is arranged to sputter upwards and the substrate holder can be heated. The sputtering system is equipped with RF power supply. The base pressure was maintained around 10^{-6} Torr. The overall gas flow is maintained at 20 sccm and all the depositions are carried out at a substrate temperature of 200ºC. Pre-heat and sputter times were preset on a count-down timer. Sputtering was started after the designated pre-sputter time had lapsed by manually opening the shutter. During the pre-sputter period, the substrate holder is pre-heated to 200ºC for 30 minutes. Aluminum nitride films were deposited by reactively sputtering Al (99.999% pure) in an argon/nitrogen gas mixture. The substrates were 1 in x 1 in silicon wafers with thermal oxide and 3 in x 1 in pieces of soda-lime glass. Electrical properties of aluminum nitride films could not be extracted because it acts as an insulator and hall effect measurements can only be done on sufficiently conductive films.

4.2 EFFECT OF GAS FLOW RATIO

Aluminum nitride thin films were deposited by reactive sputtering on thermal oxide silicon wafers and glass substrates by varying the gas flow ratio of Argon/Nitrogen. The rest of the parameters were kept constant. The index of refraction and extinction coefficient were extracted from Spectroscopic ellipsometry on Silicon with thermal oxide, as illustrated in Figure 4.1 The optical properties of AlN films were modeled using three terms Cauchy model. The Cauchy model is mainly used for insulators and semiconducting materials with wide bandgap. The parameters obtained from the ellipsometry are summarized in Table 4.1.

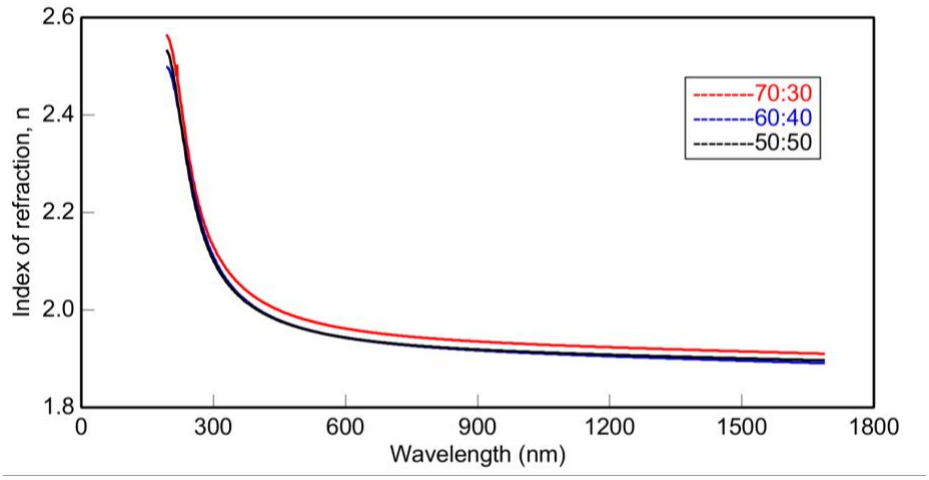

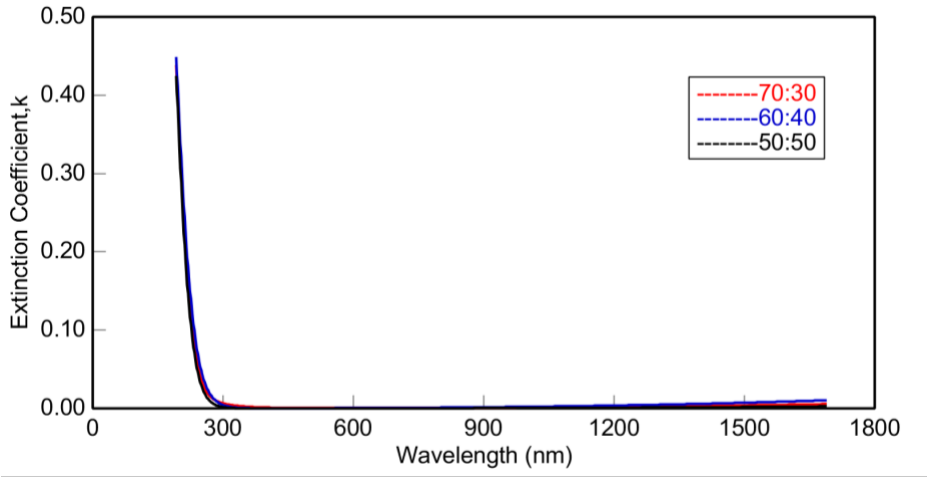

Fig. 4.1 The index of refraction, n and extinction coefficient, k extracted by spectroscopic ellipsometry as a function of varying gas flow ration Argon/Nitrogen of AlN films.

Table 4.1 Optical properties of AlN films as a function of varying gas concentration.

Gas flow ratio (A r: N2)	**Film thickness (nm)**	**Roughness (nm)**	**Index of refraction**		**Extinction coefficient**	
			@ 1240 nm	**@ 200 nm**	**@ 1240 nm**	**@ 200 nm**
70:30	67.99	4.88	1.930	2.652	2.73E-05	0.417
60:40	64.57	4.35	1.912	2.58	2.45 E-05	0.411
50:50	60.47	1.84	1.904	2.551	7.18E-05	0.368

From Figure 4.1 and Table 4.1, it is clear that there is no significant change in the optical constants as function of varying gas concentration. Nitrogen gas concentration is not increased to more than 50% with respect to argon gas, as the target will get poisoned forming an aluminum nitride layer, which will cause the sputtering yield to decrease The refractive index of the films ranges from 1.915 to 2.594. The extinction coefficient is very small, and it is close to zero at high wavelength (>700 nm) region, indicating the films are transparent in the visible region. The refractive indices of c-AlN deposited on sapphire substrates varied between 2.373-2.079 and the extinction coefficients varied between 0.106-0.08 for the wavelength range 300-800nm [23]. The values obtained for n and k are close to the crystalline AlN thin films. The difference in the values is due to the nano-crystalline structure of the deposited films. Best-fit model parameters are summarized in Table 4.2. One can observe that the values of the parameters are very close that demonstrates the validity of the Cauchy AlN thin film model.

Table 4.2 Best-fit model parameters for AlN thin films for different Gas flow ratios

Cauchy Parameters/ Gas flow ratio	A	B	C	k Amplitude	Exponent
70:30	1.922	0.01323	0.00064	0.00908	1.852
60:40	1.904	0.01331	0.00061	0.0017	1.798
50:50	1.904	0.01250	0.00059	0.00806	1.850

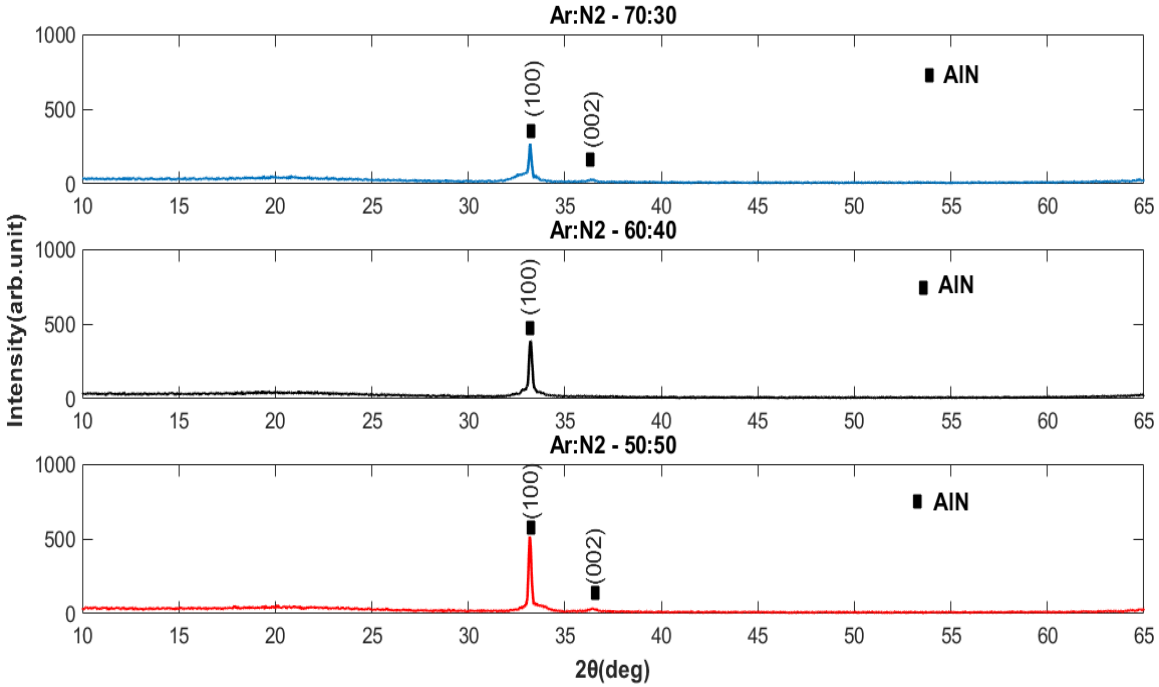

Fig 4.2 XRD spectra of the deposited Aluminum Nitride film for different gas flow ratio.

The XRD pattern of aluminum nitride films deposited on silicon wafer with thermal oxide is shown in Figure 4.2. It has been found that, for all flow ratio of nitrogen/argon, a peak can be seen around 33º, which correspond to the (100) peak of Aluminum Nitride. For nitrogen concentrations of 30% and 50%, it can be observed that a small peak starts to appear around 36.4º, which correspond to the (002) peak of Aluminum Nitride. As one can see, there is a definite

improvement in the crystallinity of the film with the increase in Nitrogen concentration, as indicated by the increase in the peak intensity. The data were further analyzed. From Table 4.3, one can observe that the FWHM is decreasing with increase in nitrogen concentration, which indicates that the film deposited at high nitrogen concentration resulted in larger crystallite sizes. There is also an increase in peak intensity, indicating a higher degree of crystallization.

Table 4.3 XRD data of deposited thin films of AlN with varying gas concentration.

Gas flow ratio (A r: N2)	**Intensity (cps)**		**FWHM (deg)**	
	(100)	**(002)**	**(100)**	**(002)**
70:30	269	33	0.22	0.49
60:40	385	-	0.21	-
50:50	515	34	0.18	0.54

Figure 4.3 shows the rate of deposition for different nitrogen/argon flows of AlN. The thickness of the films was extracted using ellipsometry. The deposition rate is calculated by dividing the thickness by the total time of deposition. It is clear that the rate of deposition continues to decline with an increase of the nitrogen/argon flow rate, because the momentum transferred due to nitrogen ion is lower when compared to the massive argon ion. Consequently, the number of sputtered atoms decrease as seen in Figure 4.3. Furthermore, due to the high concentrations of nitrogen, there is a chance of poisoning the target and the sputter yield of AlN is far less than Al, which can cause the deposition rate to decrease too.

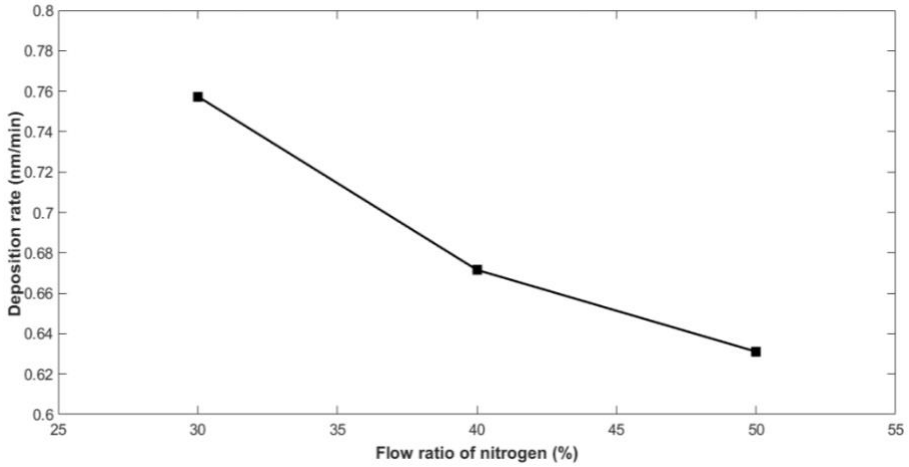

Fig 4.3 Deposition rate of AlN thin films for different nitrogen/argon flow ratio.

4.3 EFFECT OF RF POWER

Aluminum nitride thin films were deposited by reactive sputtering on silicon wafers with thermal oxide by varying the power. The power was varied from 150W-200W. The rest of the parameters were kept constant. More specifically, the nitrogen/argon ratio was set to 30 percent Nitrogen gas.

Figure 4.4 shows the X-ray diffraction patterns of AlN thin films deposited using 30 percent Nitrogen gas ratio on thermal oxide silicon wafer. All the films show a preferred orientation along the (100) orientation (around 33º). The crystallinity of the films barely changes with power change from 150 W to 175 W, with mostly an amorphous broad peak, but increases with the increase of the sputtering power to 200 W. At 200W, peaks appear with much higher intensity and reduce full width at half maximum, indicating increase content of crystalline phase as well as increased grain size. The extracted results from the XRD analysis are summarized in Table 4.4. We can observe that for 175 W, the FWHM is high that indicates the film has poor

quality with small crystallite sizes. Increase in the power, increases the kinetic energy of the ions which increases the deposition rate and, thus, the crystallinity of the films.

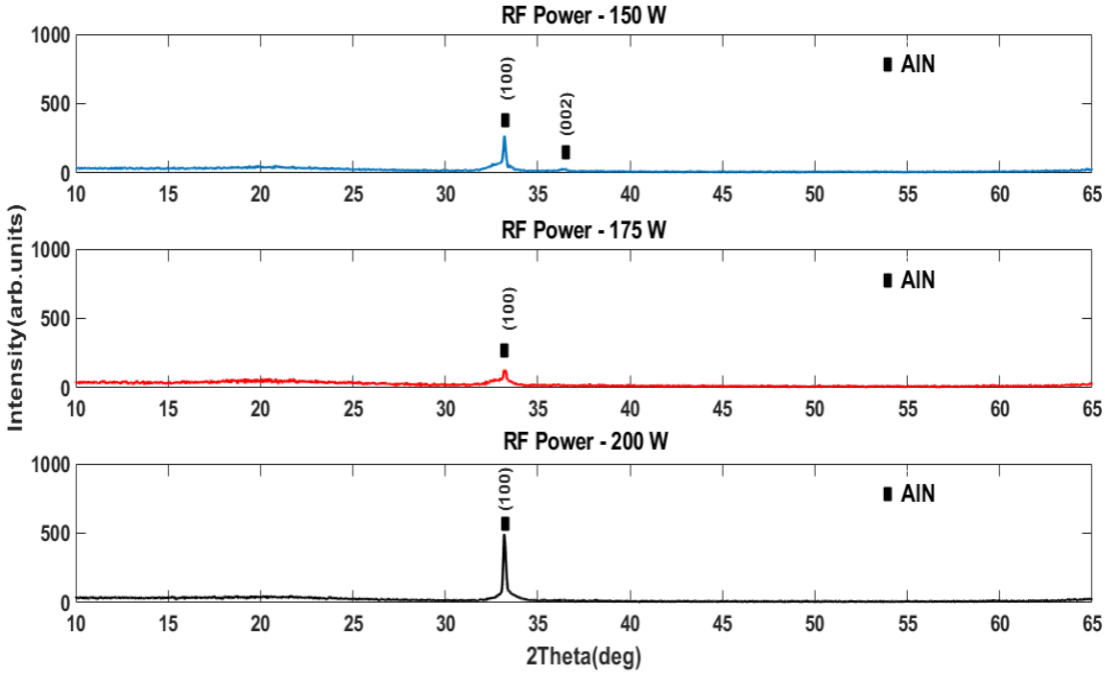

Fig 4.4 XRD spectra of the deposited Aluminum Nitride film for different sputtering power.

Table 4.4 XRD data of deposited thin films of AlN with varying RF Power

RF Power (W)	**Intensity (cps)**		**FWHM (deg)**	
	(100)	**(002)**	**(100)**	**(002)**
150	269	33	0.22	0.49
175	128	-	0.70	-
200	494	34	0.18	0.18

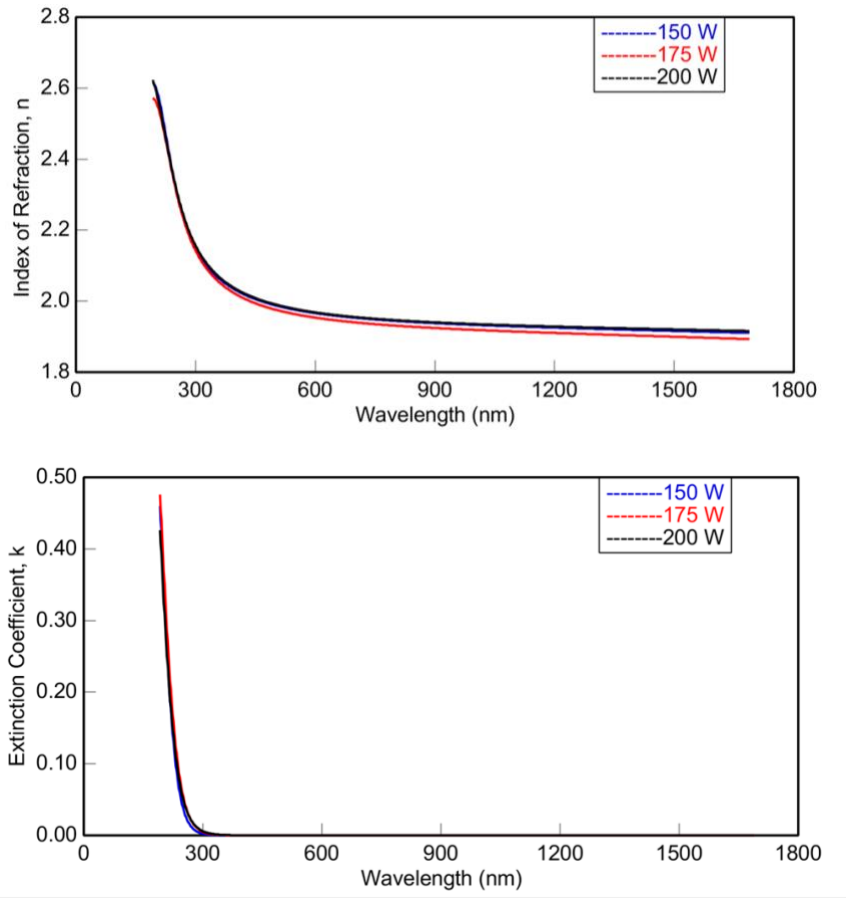

Fig. 4.5 The index of refraction, n, and extinction coefficient, k, extracted by spectroscopic ellipsometry as a function of varying RF powers for AlN films.

The index of refraction and extinction coefficient were extracted from spectroscopic ellipsometry on Silicon with thermal oxide, as illustrated in Figure 4.5. The optical properties of AlN films were generated using three terms Cauchy model. The index of refraction and extinction coefficient plotted do not show any major differences with increase in power. This suggests that the films have similar phases. Table 4.5 summarizes the best fit model parameters for varying RF power. The fitting was achieved by minimizing the mean square error (MSE). Table 4.6 summarizes the extracted film thickness, roughness, refractive index and extinction coefficient of the deposited AlN films. Overall, the refractive index of the AlN films improves as a function of

increasing plasma power, indicating an enhancement in the film quality. However, AlN grown at 175 W exhibited a slightly reduced refractive index toward longer wavelengths. Moreover, the near-zero extinction coefficient of the AlN in the visible region is also another indication of higher quality films.

Table 4.5 Best-fit model parameters of AlN thin films for different RF power

Cauchy parameters/ RF power (W)	**A**	**B**	**C**	**k Amplitude**	**Exponent**
200	1.919	0.01513	0.00056	0.01078	1.753
175	1.906	0.01537	0.00056	0.01176	1.778
150	1.922	0.01323	0.00064	0.00908	1.852

Table 4.6 Optical properties of AlN films as a function of varying RF powers.

RF Power (W)	**Film thickness (nm)**	**Roughness (nm)**	**Index of refraction**		**Extinction coefficient**	
			@ 1240 nm	**@ 200 nm**	**@ 1240 nm**	**@ 200 nm**
200	88.85	4.96	1.929	2.660	5.02E-05	0.404
175	73.70	3.48	1.910	2.567	3.31 E-05	0.3673
150	67.99	4.88	1.92	2.605	2.73E-05	0.367

4.4 EFFECT OF SPUTTERING PRESSURE

Aluminum nitride thin films were deposited by reactive sputtering on silicon wafers with thermal oxide by varying the pressure. The pressure was varied from 1 mTorr to 5 mTorr. The rest of the parameters were kept constant. More specifically, the nitrogen/argon ratio was set to 30 percent Nitrogen gas and the power was set at 200W.

The effect of variation in pressure on the optical constants extracted from ellipsometry are plotted in Figure 4.6. As one can see, the index of refraction is decreasing with increase in the pressure, while the extinction coefficient seems higher for the lower pressure.

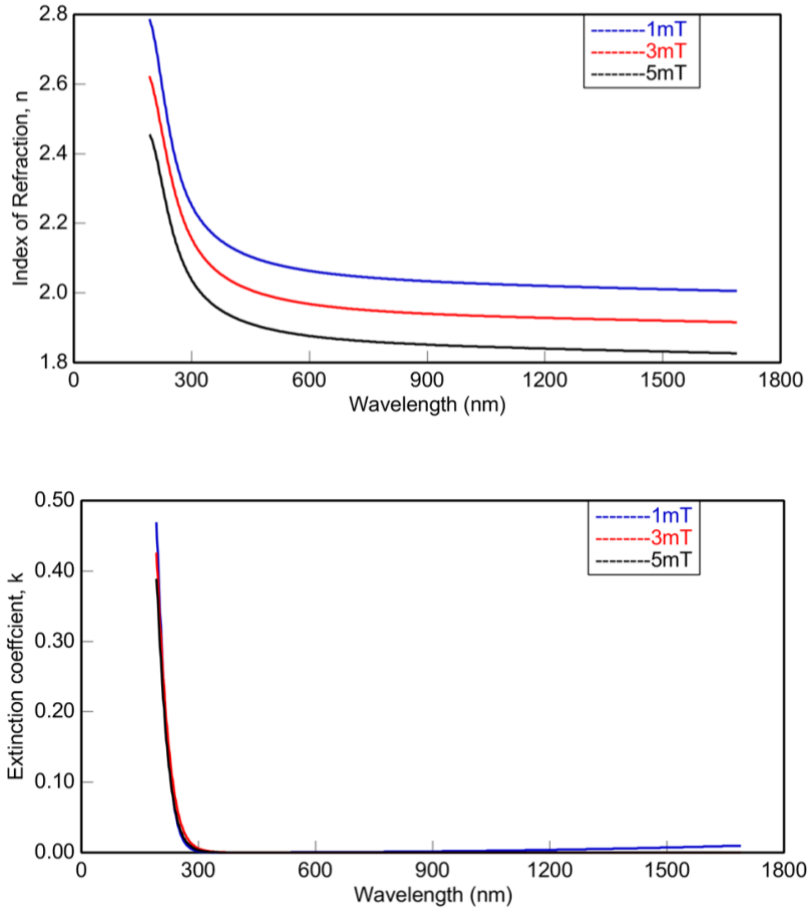

Fig. 4.6 The index of refraction, n, and extinction coefficient, k, extracted by spectroscopic ellipsometry as a function of varying Pressures for AlN films.

Table 4.7 Best-fit model parameters of AlN thin films for different sputtering pressure.

Cauchy parameters/ Pressure (mTorr)	**A**	**B**	**C**	**k Amplitude**	**Exponent**
1	2.013	0.01313	0.00073	0.00969	1.925
3	1.919	0.01513	0.00056	0.01078	1.753
5	1.839	0.01290	0.00049	0.00892	1.763

Table 4.8 Optical properties of AlN films as a function of varying sputtering pressure.

Pressure (mTorr)	**Film thickness (nm)**	**Roughness (nm)**	**Index of refraction**		**Extinction coefficient**	
			@ 1240 nm	**@ 200 nm**	**@ 1240 nm**	**@ 200 nm**
1	140.09	3.30	2.016	2.813	3.81E-05	0.412
3	88.85	4.96	1.929	2.660	5.02E-05	0.404
5	71.31	3.33	1.840	2.438	0.00221	0.293

Table 4.8 gives the best-fit cauchy model parameters and all the parameters are close, which indicates the model is valid for AlN thin films. The effect of variation in pressure on the optical constants extracted from ellipsometry are summarized in Table 4.7. The kinetic energy of

the sputtered particles decreased because of collision scattering with increasing the sputtering pressure. At a higher pressure, the atoms reaching the film surface do not have enough energy to move to a suitable location, then the film crystallinity decreases, and films became less transparent, which resulted in the decrease of reactive index.

The above results are compared with XRD data shown in Figure 4.7 and Table 4.9. It is clear from the XRD spectra that varying pressure is causing a different phase orientation, as one can see that lowering the pressure to 1 mTorr resulted in (002) orientation of AlN around 36º and (100) orientation around 33º is starting to disappear. Lower pressure is favorable for (002) orientation. It is likely that the deposited atoms may have altered their direction, energy, momentum and mobility as the mean free path of atoms increases. Increase in the pressure switched the orientation to (100) and the crystallinity decreased with the increase in pressure It can be observed that refractive indices of 3 mTorr and 5 mTorr are different which indicates the presence of a different phase. Most likely the film deposited using 5 mTorr is amorphous AlN, since XRD shows a weaker peak for that pressure. As discussed above, increase in pressure also increases the collisions between the ions and ultimately affects the crystalline quality of the films.

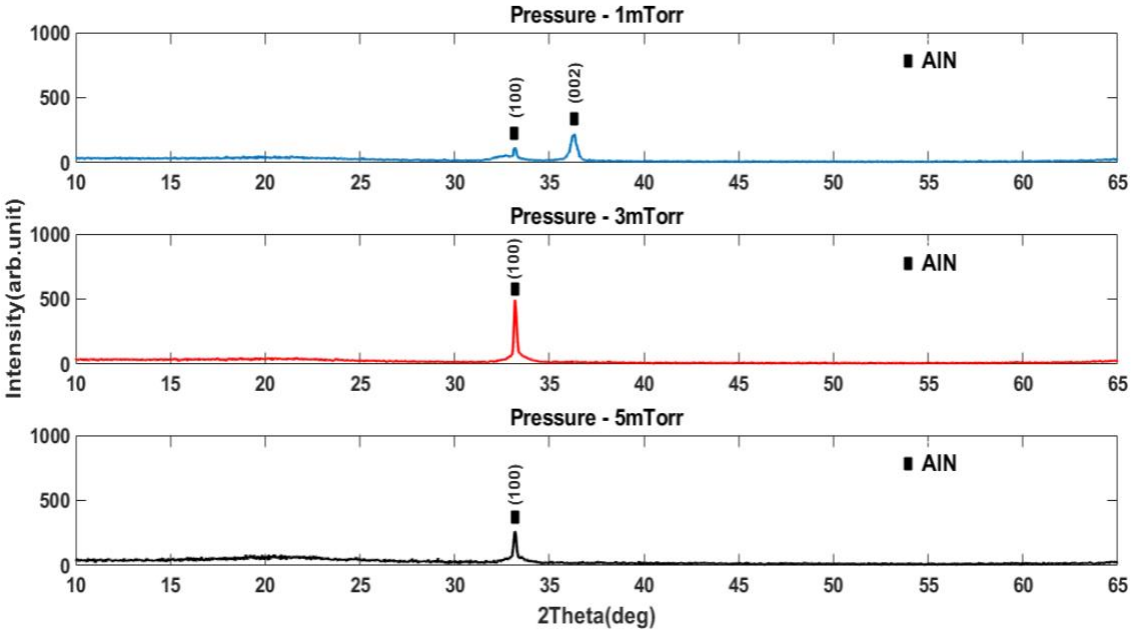

Fig 4.7 XRD spectra of the deposited Aluminum Nitride film for different pressures

Table 4.9 XRD data of deposited thin films of AlN with varying Sputtering pressure

Pressure (mTorr)	Intensity (cps)		FWHM (deg)	
	(100)	(002)	(100)	(002)
1	115	214	0.19	0.40
3	494	-	0.19	-
5	263	-	0.20	0.18

4.5 EFFECT OF SUBSTRATES

The films were deposited on two different substrates – namely silicon wafers with thermal oxide and soda-lime glass. The index of refraction, n, as well as the extinction coefficient, k, as extracted from ex-situ SE are shown in Figure 4.8 for different substrates. As one can see, the film

deposited on silicon wafer with thermal oxide have high refractive index and extinction coefficient. The optical characteristics clearly show that the films have different phase. Table 4.10 shows the best-fit parameters of the optical model. The fitting is done by minimizing the mean square error. Slight difference can be observed, which is due to the change in the substrate.

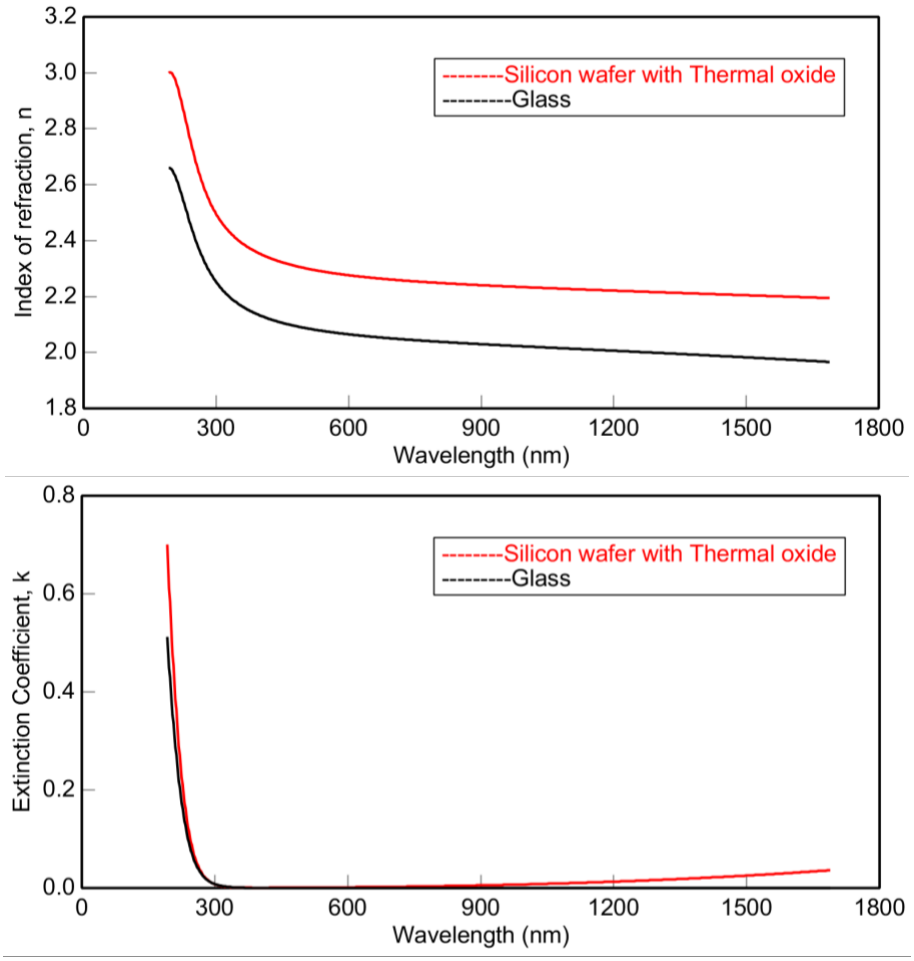

Fig. 4.8 The index of refraction, n, and extinction coefficient, k, extracted by spectroscopic ellipsometry for different substrates for AlN films

Table 4.10 Best-fit model parameters of AlN thin films for different substrates

Cauchy parameters/ Substrates	A	B	C	k Amplitude	Exponent
Glass	2.012	0.0133	0.00068	0.01290	1.813
Silicon wafer with thermal oxide	2.220	0.0138	0.00095	0.02945	1.484

The results were compared with the XRD spectra shown in Figure 4.9. It is clear from the XRD spectra that the AlN films deposited on the glass substrate did not crystallize readily. The large peak at low angle shows the background peak from the amorphous glass substrate. For the films deposited on the silicon wafer with thermal oxide, it seems that the aluminum nitride films are nanocrystalline, whereas the film deposited on glass substrates are completely amorphous. This is consistent with the results from the previous section.

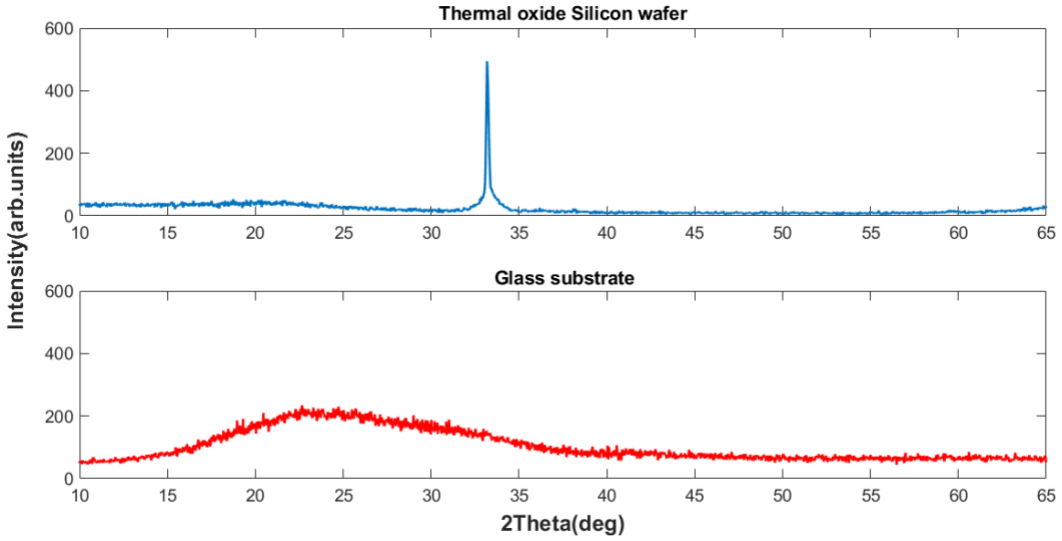

Fig. 4.9 XRD spectra of the deposited Aluminum Nitride film on different substrates

4.6 CONCLUSION

In this chapter, Aluminum nitride thin films were deposited by reactive RF magnetron sputtering on various substrates. The effect of Gas flow ratio, sputtering power, pressure and substrates were studied. It was observed that the Nitrogen gas flow ratio of at least 50%, with a power of 200W was necessary to deposit nanocrystalline films. Lowering the Pressure to 1 mTorr is resulting in c-axis oriented AlN. It was also observed that films deposited on silicon wafer with thermal oxide led to higher crystalline phase compared to glass substrates.

CHAPTER 5

EFFECT OF SPUTTERING PROCESS PARAMETERS ON INDIUM NITRIDE THIN FILMS GROWTH

5.1 PROPERTIES OF INDIUM NITRIDE

Indium nitride (InN) is a small bandgap material which has potentials applications in optics. It has a bandgap around 0.7 eV. InN has been shown to have the lowest effective mass among the III-nitride semiconductors. This low effective mass value results in a high mobility and high saturation velocity of the electrons and hence a potential in high speed devices. The lattice constants are 3.545 Å for the a-axis, and 5.703 Å for the c-axis. InN, like other group-III nitrides, has lower c/a ratio than the ideal value of 1.633 [25]. The refractive index of indium nitride is around 2.9 in the visible. Undoped InN has a high electron concentration, leading to a n-type conductivity. The use of InN and its alloys with GaN and AIN allows tuning of the band gaps and emission wavelengths from the deep ultraviolet to the near infrared, which may be useful for a variety of applications. Indium nitride crystalizes in the stable forms of wurtzite and zinc blende and exists in a rock salt form. The transitions of the wurtzite phase to the rock salt were observed at high hydrostatic pressures. [26].

The most difficult of all III-nitrides has been InN growth technology. The first problem with InN epitaxy was the lack of matching substrates, resulting in defects and dislocations. InN thermal decomposition starts at temperatures over 470 °C, which poses the second problem. InN can be used in solar cell when alloyed with Gallium, forming a ternary alloy system [27]. With bandgap energies ranging from 0.7 eV for InN to 3.4 eV for GaN, this one ternary material system could span almost the entire solar spectrum (0.4 to 4.0 eV). Not only solar cells but the applications

of this ternary alloy can be extended to LED's and lasers just by tuning the bandgap. InN can be used as a low resistivity layer for ohmic contact formation to other wider band gap nitrides.

Sputter parameters for the indium nitride thin films

An AJA Orion 8 sputtering system with a KDC-40 ion beam controller was used. The target is arranged to sputter upwards and the substrate holder can be heated. The sputtering system is equipped with a RF power supply. The base pressure was maintained around 10^{-6} Torr. The overall gas flow is maintained at 20 sccm and all the depositions are carried out at room temperature, contrarily to the AlN deposition because of the potential for decomposition at high temperature. Pre-heat and sputter times were preset on a count-down timer. Sputtering was started after the designated pre-sputter time had lapsed by manually opening the shutter. Indium nitride thin films were deposited by reactively sputtering In (99.999% pure) in an argon/nitrogen gas mixture. The substrates were 1 in x 1 in silicon wafers with thermal oxide and 3 in x 1 in soda-lime glass slides.

5.2 EFFECT OF GAS FLOW RATIO

Indium nitride thin films were deposited by reactive sputtering on silicon wafers with thermal oxide by varying the gas flow ratio of Argon/Nitrogen More specifically, the sputtering pressure was set to 1 mTorr and the power was set at 80 W. Figure 5.1 shows the XRD patterns of Indium Nitride films deposited on Silicon wafer with thermal oxide at various gas concentrations. Table 5.1 summarized the XRD data. A nanocrystalline structure is clearly observed for all InN films deposited at room temperature. Many peaks were observed, belonging to the hexagonal InN structure, notably the (100), (002), (101), (110), (112) and (103) peaks. At higher Ar:N_2 ratio (60:40 and 80:20), the intensity of the (101) crystalline peak was high. Increase in nitrogen concentration resulted in (002) preferred orientation. For a decrease in the Nitrogen concentration

and increase in the Argon flow with 80:20 Ar:N_2 ratio, smaller peaks corresponding to the indium metal are detected in the XRD pattern, which is probably due to the lack of nitrogen to react with In, leading to slightly In-rich conditions.

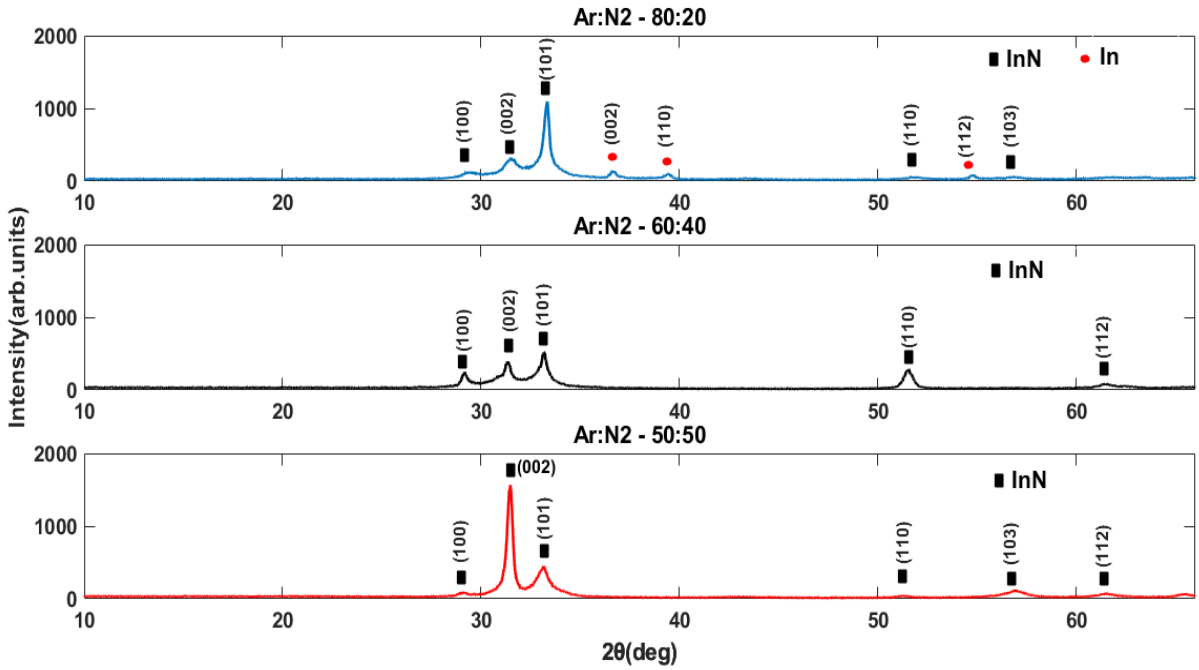

Fig. 5.1 XRD spectra of InN films as a function of gas flow ratio

The FWHM of the peak around 31.4 is decreasing with increase in the nitrogen concentration, which indicates that the films deposited at 50% nitrogen have larger crystallite sizes along the (002) orientation.

Table 5.1 XRD data of deposited thin films of InN with varying gas concentration.

Orientation (hkl)	Intensity(cps)			FWHM (deg)		
	80:20	**60:40**	**50:50**	**80:20**	**60:40**	**50:50**
100	133	248	-	0.69	0.37	-
002	31	368	1568	0.76	0.44	0.27
101	1083	519	424	0.33	0.30	0.73
110	50	286	41	1.01	0.50	0.81
103	51	-	107	1.37	-	1.23
112	-	76	81	-	1.21	1.21

The above results can be compared with the refractive index data in Figure 5.2, extracted from spectroscopic ellipsometry. A general oscillator model with three oscillators, namely Drude and 2 CPPB oscillators, were used to fit the data with minimum error. The ellipsometry data of Ar:N_2- 80:20 could not be extracted because the surface was too rough. The difference in the index of refraction is indicating the presence of a different phase, that can also be observed in the XRD data. InN film deposited with 50 % concentration of nitrogen has a peak around 57º which is due to (103) orientation and that peak is also not observed in the film deposited with 40% Nitrogen concentration. Also, the crystalline quality of film deposited with Ar:N_2- 50:50 is higher than the one with Ar:N_2- 60:40, which contributes to the difference in the index of refraction.

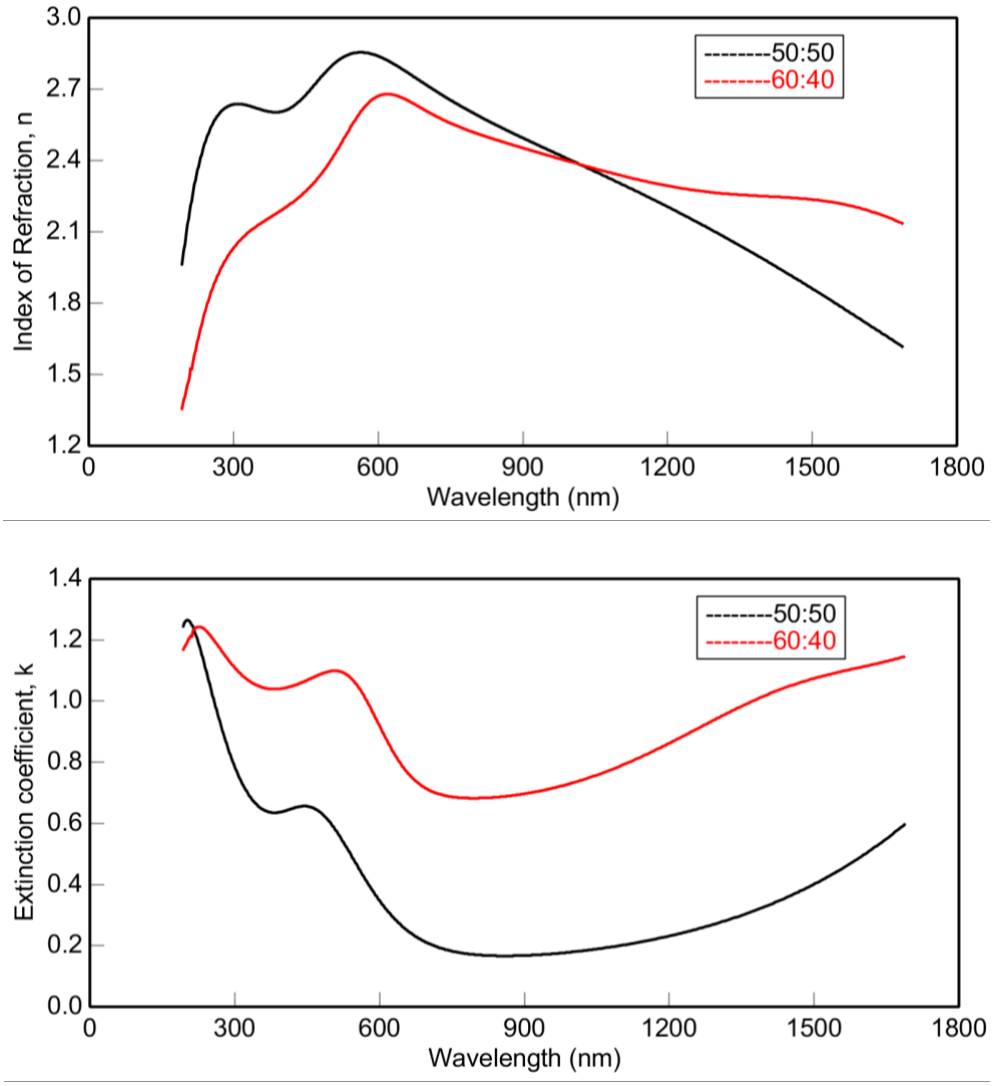

Fig. 5.2 The index of refraction, n, and the extinction coefficient, k, as a function wavelength when varying gas flow ratios Argon/Nitrogen for InN films.

Table 5.2 Optical properties of InN films as a function of with varying gas concentration.

Gas flow ratio (A r: N2)	**Film thickness (nm)**	**Resistivity (ohm.cm)**	**Index of refraction**		**Extinction coefficient**	
			@ 1240 nm	**@ 500 nm**	**@ 1240 nm**	**@ 500 nm**
50: 50	580.28	5.12E-04	2.16	2.79	0.246	0.597
60:40	562	3.35E-04	2.27	2.39	0.894	1.098

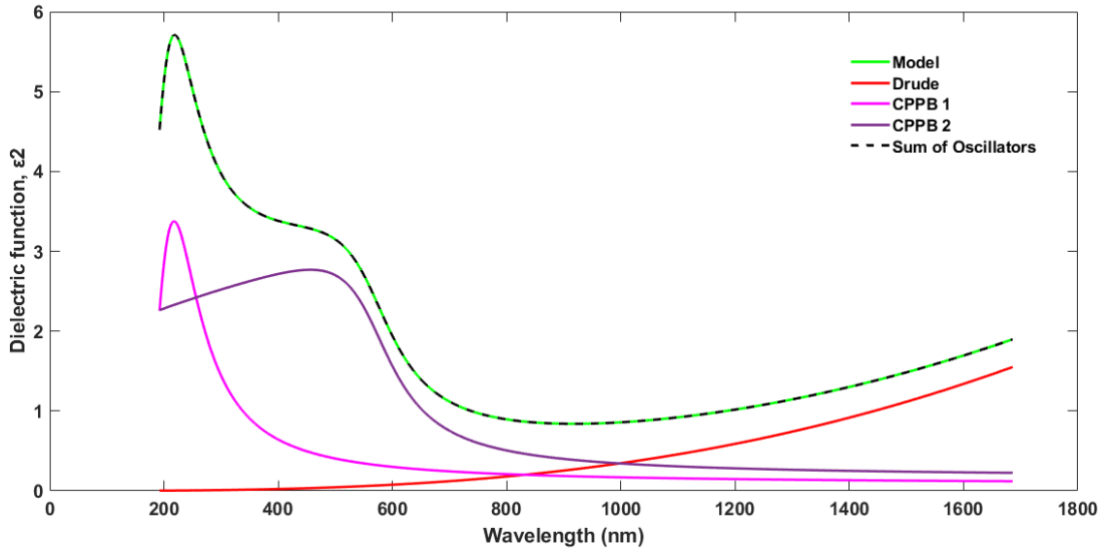

Fig 5.3 Sum of oscillators to describe optical model of InN film deposited at 50:50 gas ratio.

Table 5.3 CP Energies as well as broadening of CPs for InN thin films for different gas flow.

Gas flow ratio	**50: 50**		**60:40**	
	E_1	**E_2**	**E_1**	**E_2**
Broadening (eV)	2.204	0.5586	3.5777	0.57
CP energies (eV)	6.104	2.155	5.029	2.070

From the Table 5.2, one can see that at higher Ar:N2 ratio because the percentage of nitrogen is low, it results in indium-rich films. The incorporation of indium causes the decrease in resistivity. The extinction coefficient is non-zero, which means that the films are not transparent. The refractive index has its maximum value 2.87 at the wavelength of 600 nm and the values are varying from 2.08 to 2.24 in the range of 300-1400 nm. The maximum value of the refractive index

obtained is in good agreement with that reported by Tyagai et al. (3.12) [24]. Figure 5.3 shows the imaginary dielectric function which is deconvoluted into three oscillators. The broadening of the CP oscillator is generated by photons interacting with phonons and other scatterers. Thus, grain boundaries can cause such changes in the broadening term. Therefore, the grain size of InN films with different nitrogen gas percentage can be compared by comparing the broadening of the peaks, as long as the temperature is kept constant which is the case here. A small grain implies a short time for an excited carrier to reach and to be scattered by its boundary. This causes a limitation of the excited-state lifetime and thus broadens the excited-state energy. Table 5.3 summarizes the critical point energies given by the best fit of the oscillators. Broadening of E_1 and E_2 is increasing, with the decrease in nitrogen concentration. Since the broadening is decreasing with increasing nitrogen gas concentration, one can say that the crystallinity increases. Grain size can be extrapolated from XRD measurements using Scherrer's formula. The FWHM of the (002) peak (Figure 5.1) is 0.76, 0.44, and 0.27 for nitrogen gas percentage of 20, 40, and 50 respectively. This decrease in the FWHM with increasing nitrogen gas percentage indicates an increase in the grain size, supporting the results obtained by ellipsometry.

5.3 EFFECT OF RF POWER

InN thin films were deposited on silicon wafer with thermal oxide by varying the sputtering power from 80 W to 50 W. Since indium has a low melting point, the power applied to the indium target has to be kept low. The XRD patterns of InN at different sputtering powers are shown in Figure 5.4. The figure shows various peaks for the InN deposited at 50 W, all attributed to the InN crystal structure, notably the (100), (002), (101), (102), (110), (103), and (112). By increasing the sputtering power to 65 W, the intensities of the InN peaks slightly increase. When the sputtering power increases to 80 W, the intensities of the InN peaks along the (002) and (112) directions are

increasing, while the rest of the intensities decreased. The increase in crystallinity with increase in power is due to the fact that the energy of sputtered atom, which is obtained from the positive ions colliding to target, will increase with increasing sputtering power. Thus, the energy of the sputtered atom arriving at the substrate increases with increasing sputtering power to 80 W and facilitates further crystallization, resulting in the strong (101) preferred orientation. From Table 5.4, the high intensity and low FHWM of the diffraction peak for the film deposited at 80 W indicates better crystallinity.

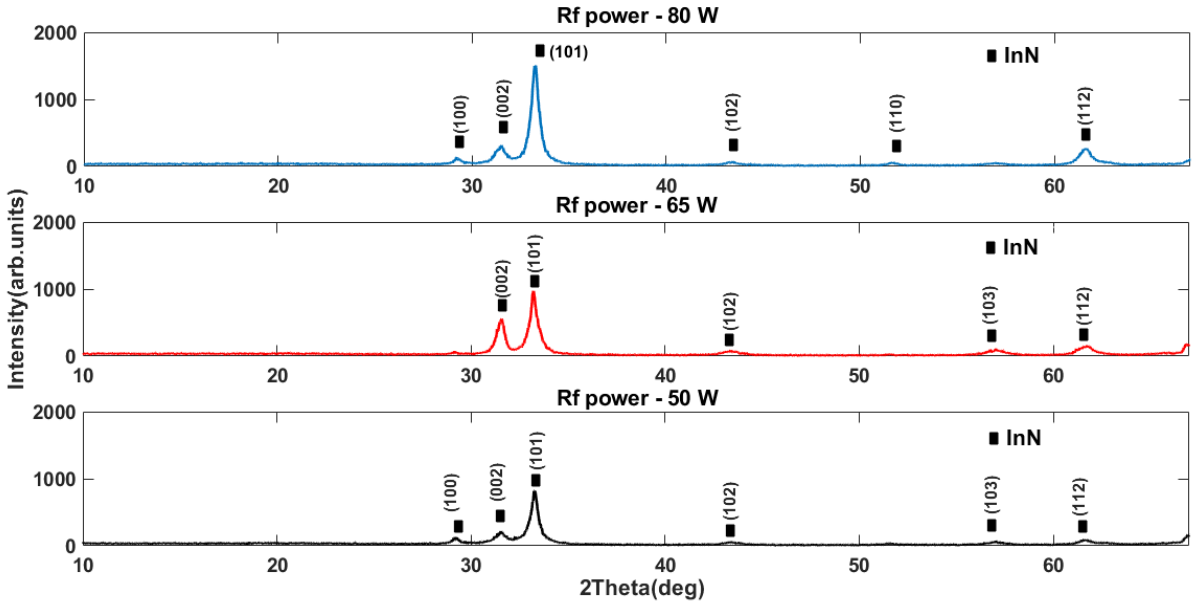

Fig. 5.4 XRD spectra of InN films as a function of sputtering power

Table 5.4 XRD data of deposited thin films of InN with varying RF Power

Orientation (hkl)	Intensity(cps)			FWHM (deg)		
	80W	65W	50W	80W	65W	50W
100	12	-	130	0.37	-	0.41
002	308	556	198	0.53	0.45	1.77
101	1507	951	810	0.51	0.57	0.52
102	76	75	58	0.70	1.06	0.87
110	56	-	38	0.48	-	0.70
103	-	57	60	-	1.18	1.24
112	268	61	85	0.87	1.07	0.92

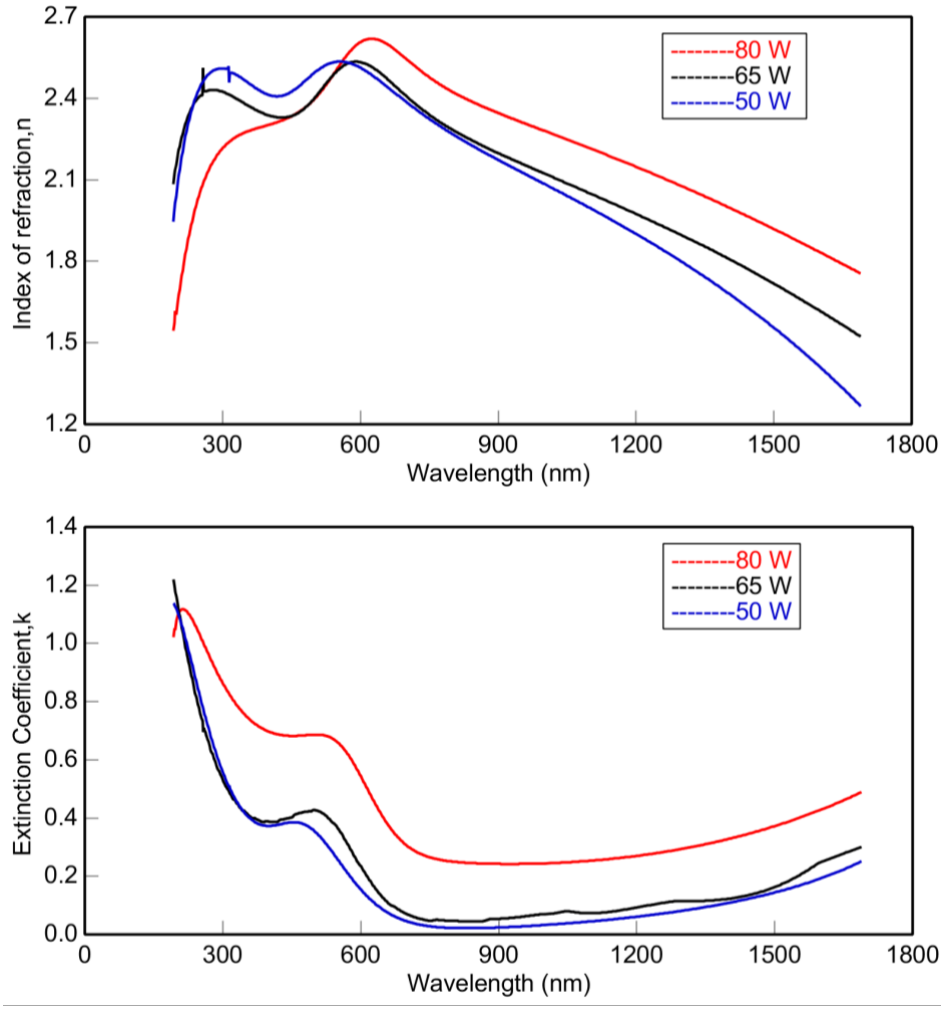

Fig. 5.5 The index of refraction, n, and extinction coefficient, k, extracted by spectroscopic ellipsometry as a function of varying RF powers for InN thin films.

Table 5.5 Optical properties of InN films as a function of varying RF Power

RF Power (W)	**Film thickness (nm)**	**Resistivity (ohm.cm)**	**Index of refraction**		**Extinction coefficient**	
			@ 1240 nm	**@ 500 nm**	**@ 1240 nm**	**@ 500 nm**
80	729	1.18E-03	2.12	2.39	0.278	0.687
65	551.8	1.19E-03	1.94	2.40	0.103	0.427
50	397.19	0.96E-03	1.86	2.49	0.068	0.354

The optical properties of InN films at room temperature were investigated using spectroscopic ellipsometry. The n and k coefficients are plotted against wavelength, as shown in Figure 5.5. As one can see the optical properties of the films deposited at 65W and 50W look similar, whereas the properties of the films deposited at 80W are different from the rest. The difference is because of the increased crystallinity of the films with increase in power. The films deposited at 80W have better crystalline quality, as seen from XRD. From Table 5.5, the index of refraction at two different wavelengths did not change much. The films deposited at 65 W and 50 W are visibly transparent due to their low thickness and it can be observed that the extinction coefficient is almost zero, which also indicates the films are slightly transparent. The resistivity of the film deposited at 50 W is slightly high, which is due to the decrease in thickness. As discussed above, the decrease in thickness is due to the deposition rate, which decreases with power.

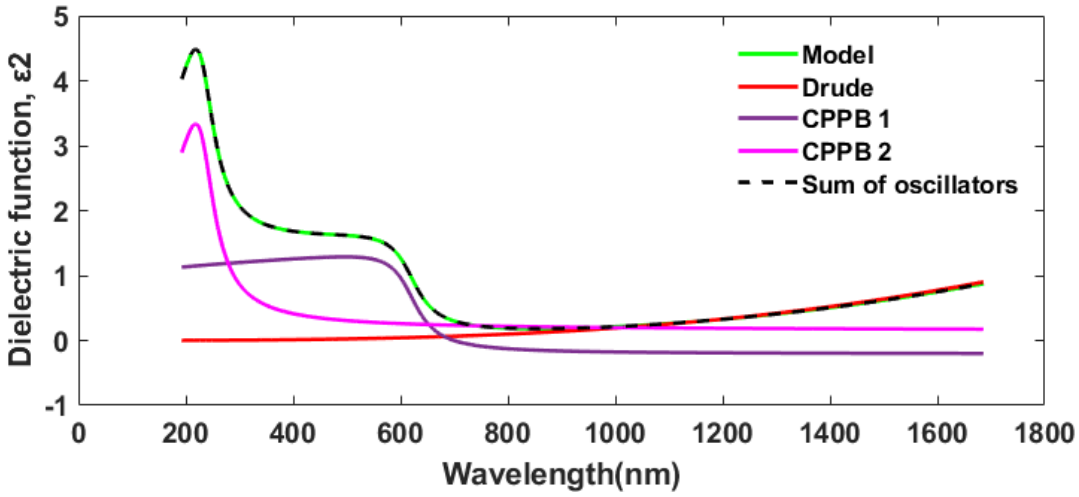

Fig 5.6 Sum of oscillators to describe the optical model of InN film deposited at 65 W.

Figure 5.6 shows the imaginary dielectric function which is deconvoluted into three oscillators. The broadening of the CP oscillator is generated by photons interacting with phonons and other scatterers. Thus, grain boundaries can cause such changes in the broadening term.

Therefore, the grain size of InN films with different RF powers can be compared by comparing the broadening of the peaks, as long as the temperature is kept constant which is the case here. Smaller grain size causes a limitation of the excited-state lifetime and thus broadens the excited-state energy. Table 5.6 gives the critical points of the best fit of the oscillators. There is not any significant shift in the Energies position for InN when the power is varied from 80 W to 50 W. Broadening of E_1 and E_2 is decreasing from 80 W to 65 W and again starts increasing with the decrease in power 50 W. Larger grains are formed when the films are deposited at 65 W RF power. Grain size can be extrapolated from XRD measurements Scherrer's formula. The broadening in the diffraction peak is not only due to the particle size but also to inhomogeneous strain or instrumental effects. Due to these effects, the particle size can be larger than the one predicted from the Scherrer's formula, which predicts only the lower limit of the particle size. The

FWHM of the (002) peak (Figure 5.4) is 0.53, 0.45, and 1.77 for RF powers of 80 W, 65 W, and 50 W respectively. This decrease in the FWHM with decrease in power to 65 W, indicating an increase in the grain size, supports the results obtained by ellipsometry.

Table 5.6 CP Energies as well as broadening of CPs for InN thin films for different RF power

RF power (W)	**80**		**65**		**50**	
	E_1	**E_2**	**E_1**	**E_2**	**E_1**	**E_2**
Broadening (eV)	0.50	1.42	0.24	1.35	0.89	2.55
CP energies (eV)	1.91	4.67	1.99	5.26	2.06	5.15

Electrical parameters were extracted from Hall effect measurements and are plotted in Figure 5.7. The figure below compares the bulk concentration, mobility, and conductivity for the different sputtering powers. One can see that the conductivity increases by a factor of 3 when going from 50 W to 80 W, indicating a better quality of the films for 80W, consistent with the XRD results.

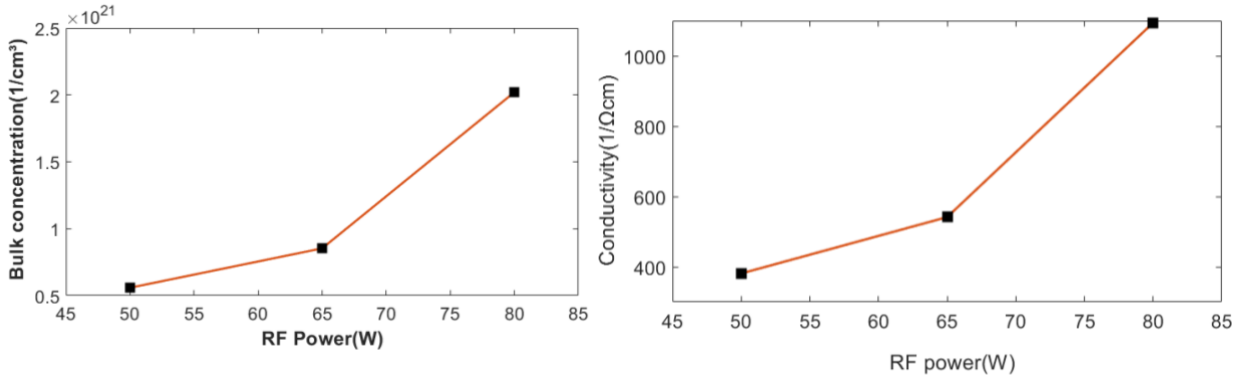

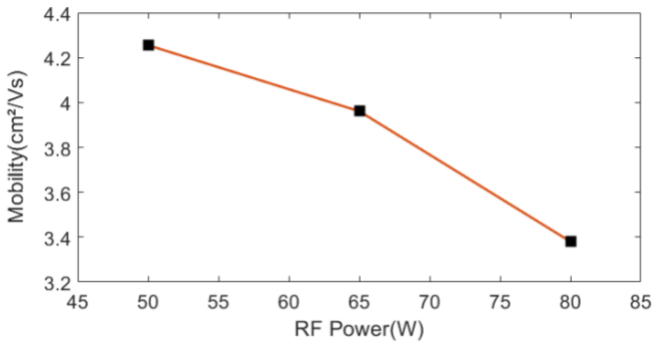

Fig. 5.7 Influence of sputtering power on electrical properties of the InN films

5.4 EFFECT OF SPUTTERING PRESSURE

InN films were deposited on silicon wafer with thermal oxide by varying the sputtering pressure from 1 mTorr to 5 mTorr, while maintaining RF power and gas flow ratio at 80 W and 60:40 (Ar: N2) respectively. Figure 5.8 shows the XRD patterns and Table 5.7 shows summarized XRD data of the InN films deposited at various sputtering pressures. The figure shows the (100), (002), (101), (110), and (112) orientations of InN, for films deposited at 1 mTorr. By increasing the sputtering pressure to 3 mTorr, the orientation of the film is switched from (002) to (101) and further increasing the pressure to 5 mTorr showed two major peaks remain, the (002) and (101). Except for the (002) and (101) directions, the rest of the peaks did not change significantly with pressure. Lower pressure resulted in higher crystalline (002) oriented InN films. It is likely that the deposited atoms may have altered their direction, energy, momentum and mobility as the mean free path of atoms increases.

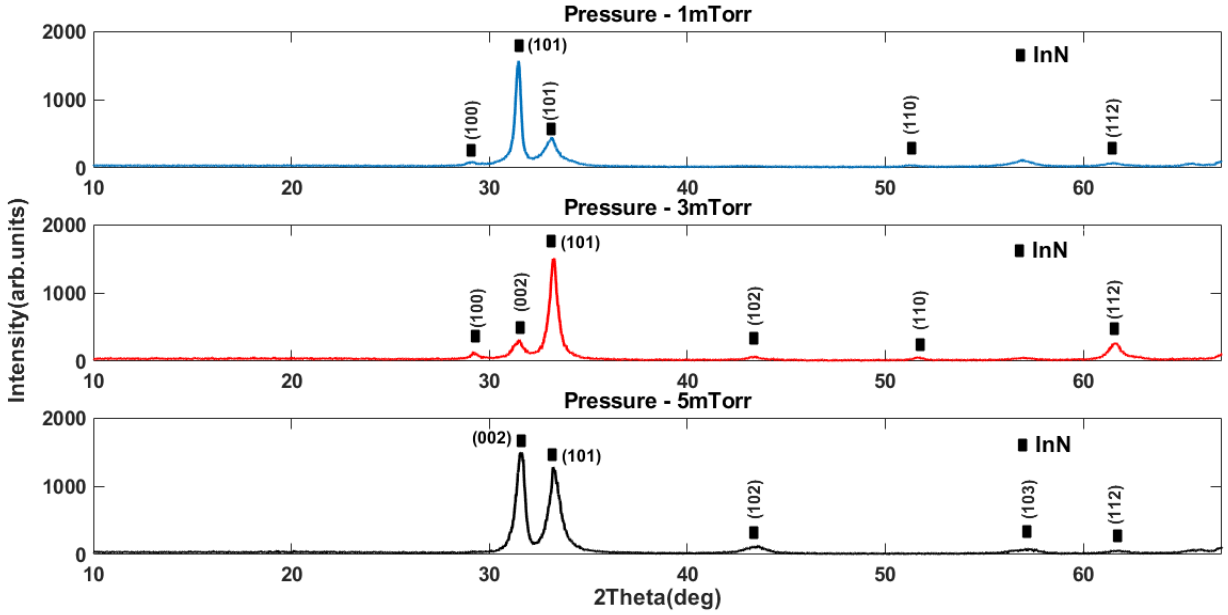

Fig. 5.8 XRD spectra of InN films as a function of sputtering pressure

Table 5.7 XRD data of deposited thin films of InN with varying pressure

Orientation (hkl)	Intensity(cps)			FWHM (deg)		
	1 mTorr	3 mTorr	5 mTorr	1 mTorr	3 mTorr	5 mTorr
100	248	12	-	0.37	0.37	-
002	368	308	1490	0.27	0.53	0.51
101	519	1507	1257	0.73	0.51	0.69
102	-	76	125	0.81	0.70	1.27
110	286	56	-	1.23	0.48	-
103	-	-	85	1.21	-	1.44
112	76	268	60	0.27	0.87	1.14

The influence of the pressure on the electrical properties on the InN film is shown in Figure 5.9. The mobility of the films tends to be slightly higher at lower sputtering pressure, indicating slightly higher quality of the films.

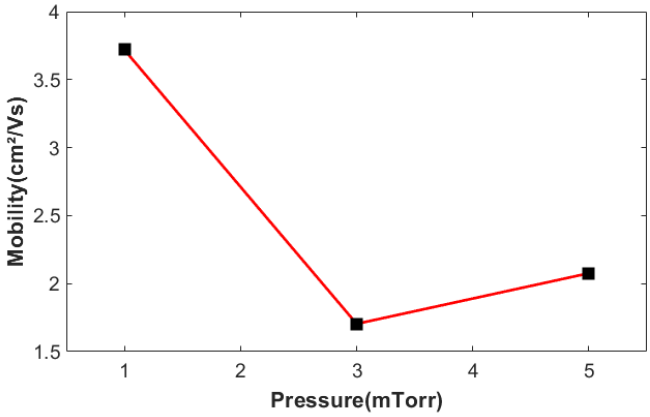

Fig. 5.9 Influence of sputtering pressure on the electrical mobility of the InN film.

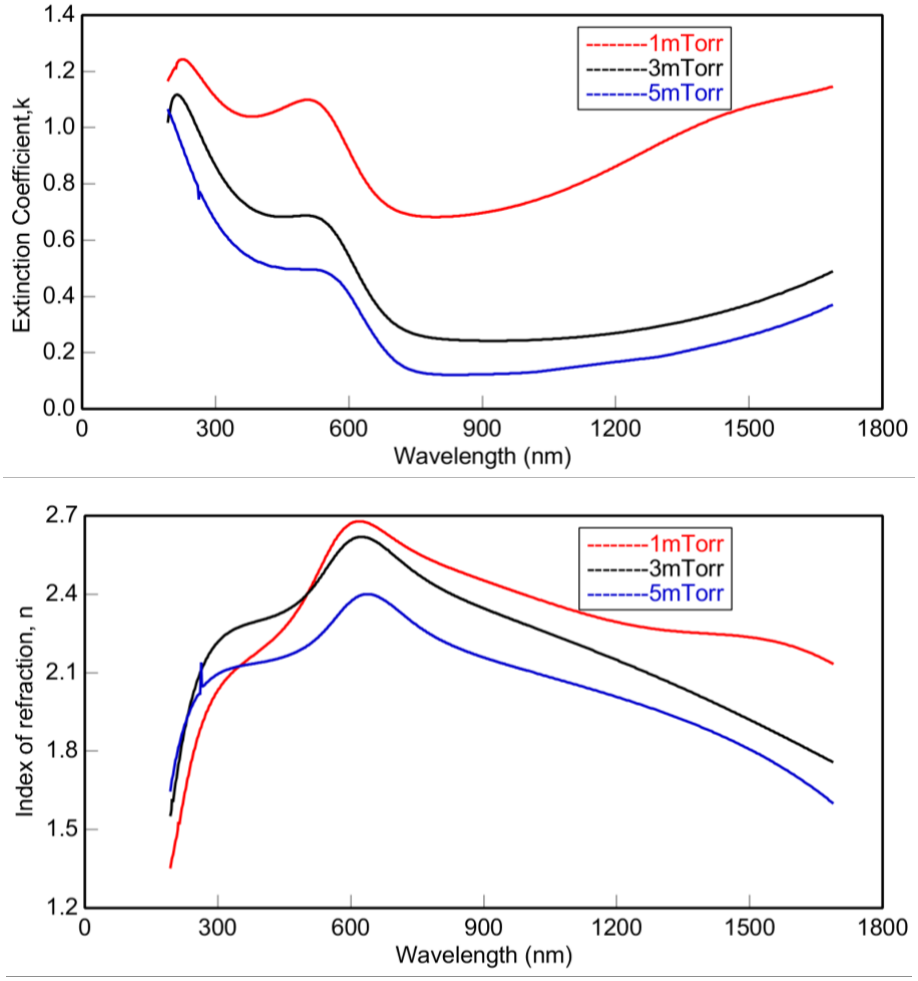

Fig. 5.10 The index of refraction, n, and extinction coefficient, k, extracted by spectroscopic ellipsometry as a function of varying Pressures for InN films.

Table 5.8 Optical properties of InN films as a function of with varying Pressure.

Pressure (mTorr)	Film thickness (nm)	Resistivity (ohm.cm)	Index of refraction		Extinction coefficient	
			@ 1240 nm	@ 500 nm	@ 1240 nm	@ 500 nm
1	562	3.35E-04	2.27	2.39	0.894	1.098
3	729	1.18E-03	2.12	2.39	0.278	0.687
5	670.22	1.30E-03	1.98	2.20	0.174	0.495

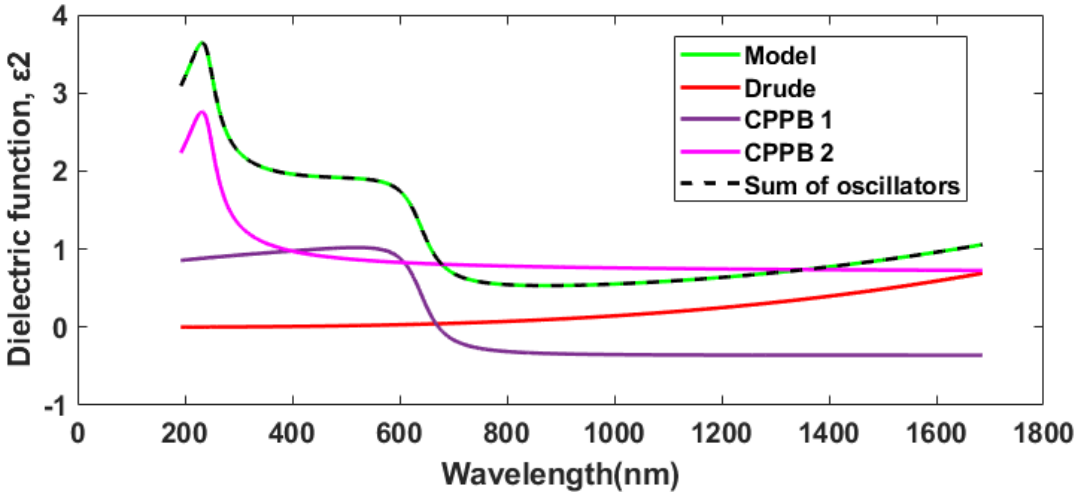

Fig 5.11 Sum of oscillators to describe the optical model of InN film deposited at 5 mTorr pressure.

Table 5.9 CP Energies as well as broadening of CPs for InN thin films for different pressure

Pressure (mTorr)	1		3		5	
	E_1	E_2	E_1	E_2	E_1	E_2
Broadening (eV)	0.57	3.57	0.89	2.55	0.22	0.85
CP energies (eV)	2.07	5.02	1.91	4.67	1.93	5.09

Figure 5.10 shows the optical constants n and k, for InN samples. The refractive index, n, varied from 2.2 to 1.9, in the range of 300 nm - 1300 nm and the maximum refractive index of 2.7 is occurring around 600 nm. Extinction coefficient of the films are in the range of 1.09-0.17, which indicates the films are not transparent. Especially films deposited at 1 mTorr are visibly opaque when compared with the other films and that is the reason for the extinction coefficient to be high. Overall, the higher sputtering pressure increases the collisions between the ions and decreases the kinetic energy of the ions which causes the growth rate to decrease and ultimately affects the crystalline quality of the films. The films at lower pressure have slightly better crystallinity with only one main orientation, which enhances the properties of the films. Figure 5.11 shows the imaginary dielectric function which is deconvoluted into three oscillators. The broadening of the CP oscillator is generated by photons interacting with phonons and other scatterers. Thus, grain boundaries can cause such changes in the broadening term. Therefore, the grain size of InN films with different sputtering pressure can be compared by comparing the broadening of the peaks, as long as the temperature is kept constant which is the case here. Smaller grain size causes a limitation of the excited-state lifetime and thus broadens the excited-state energy.

Table 5.9 shows the CP energies and broadening obtained from the best fit of the oscillators. There is not any significant shift in the Energies position for InN when the sputtering pressure is varied from 1 mTorr to 5 mTorr. Broadening of E_1 is increasing up to 3 mTorr and again starts decreasing to 5 mTorr, whereas the broadening of E_2 is decreasing when the pressure is varying from 1 mTorr to 5 mTorr. Grain size can be extrapolated from XRD measurements using Scherrer's formula. The broadening in the diffraction peak is not only due to the particle size but also to inhomogeneous strain or instrumental effects. Due to these effects, the particle size can be larger than the one predicted from the Scherrer's formula, which predicts only the lower limit

of the particle size. The FWHM of the (002) peak (Figure 5.8) is 0.44, 0.53, and 0.51 for pressures 1 mTorr, 3 mTorr, and 5 mTorr respectively. The results obtained from XRD, supports the results obtained by ellipsometry.

5.5 EFFECT OF SUBSTRATES

InN films were deposited on two different substrates – namely glass and silicon wafers with thermal oxide. The power, pressure and gas flow ratio are maintained at 80 W, 0.5 mTorr and 100% nitrogen gas respectively. Electrical parameters were extracted from Hall effect measurements and are plotted in Figure 5.12. The figure below compares the bulk concentration, mobility, and conductivity for the different substrates. As one can see that films deposited on silicon wafers with thermal oxide show superior electrical properties than those deposited on glass substrates. Films on silicon wafer with thermal oxide tend to be more crystalline than the films on glass. High crystalline quality means a fewer number of grain boundaries which will increase mobility and in turn increase the conductivity of the film.

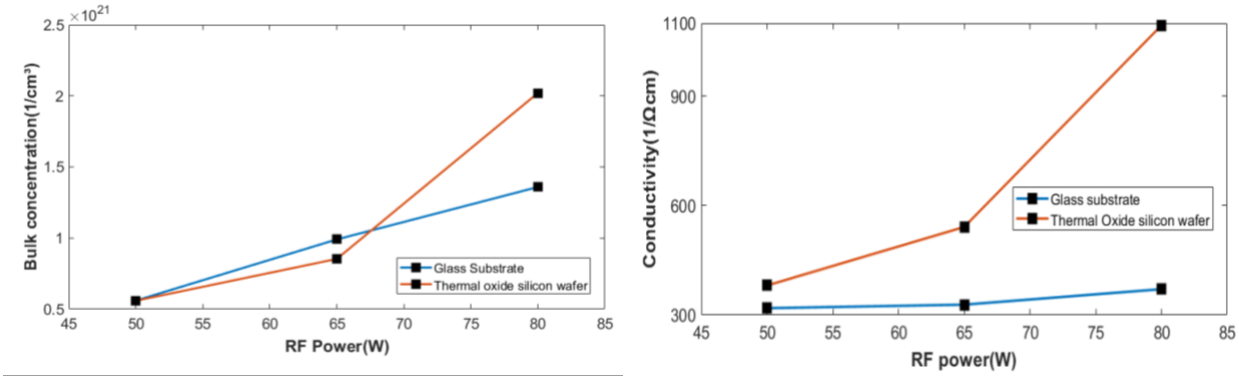

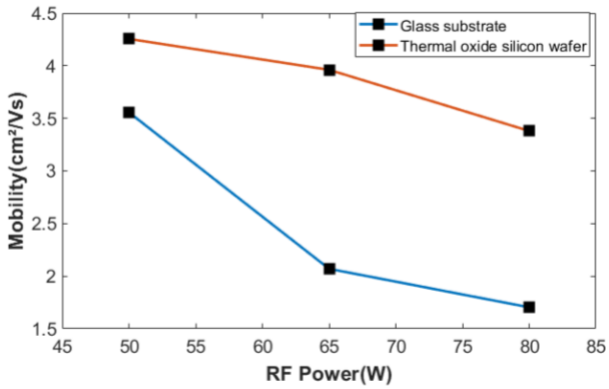

Fig. 5.12 Influence of substrates on the electrical properties of the InN films

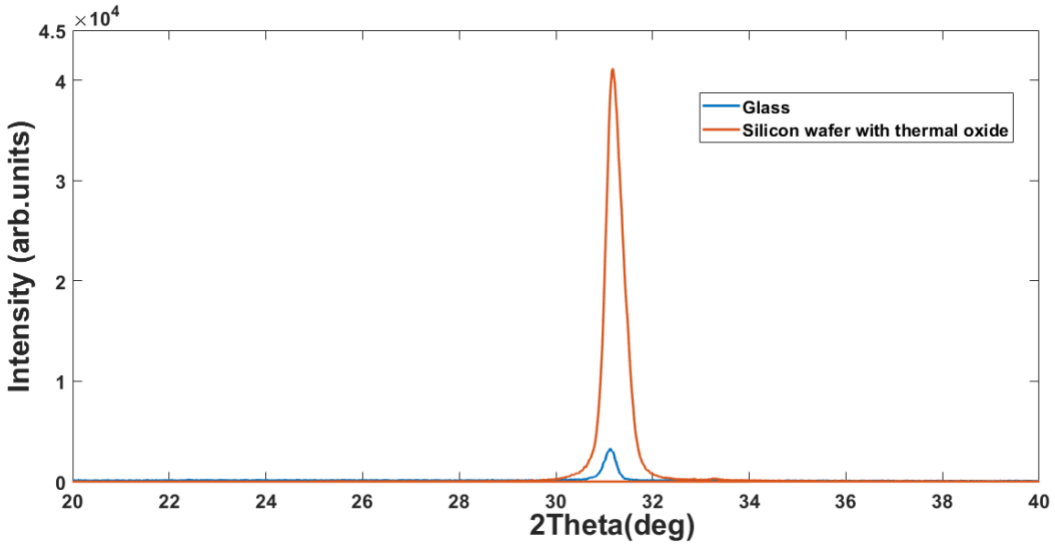

Fig 5.13 XRD spectra of the deposited Indium Nitride film on different substrates

Figure 5.13 shows the XRD of InN thin films deposited on glass and silicon wafer with thermal oxide, while maintaining RF power, Pressure and gas flow ratio at 80 W, 0.5mTorr and 100 % nitrogen respectively. As one can see, the films deposited on glass and silicon wafer with thermal oxide have only one major peak around 31º. High crystalline quality films are deposited on silicon wafer with thermal oxide and the results obtained from the XRD is consistent with the above section.

The optical characteristics of indium nitride films on various substrates are plotted Figure 5.14. A slight change in the index of refraction and extinction coefficient with substrate is observed. The film deposited on silicon wafer with thermal oxide have high refractive index indicating high crystalline quality. Similar phases are in presence for both films according to the XRD and ellipsometry plots. The change in optical characteristics can be attributed to difference in crystallinity. Table 5.10 shows the central point energies obtained from the best fit of the oscillators. The position of the central point energies did not vary much with substrates. The broadening parameter is increased for glass when compared to silicon wafer with thermal oxide.

Grain boundaries can cause such changes in the broadening term. Therefore, the grain size of InN films with different substrates can be compared by comparing the broadening of the peaks, as long as the temperature is kept constant which is the case here. The FWHM of the films deposited silicon wafer with thermal oxide is smaller than the one deposited on the glass substrate. This decrease in the FWHM indicates an increase in the grain size, supporting the results obtained by ellipsometry.

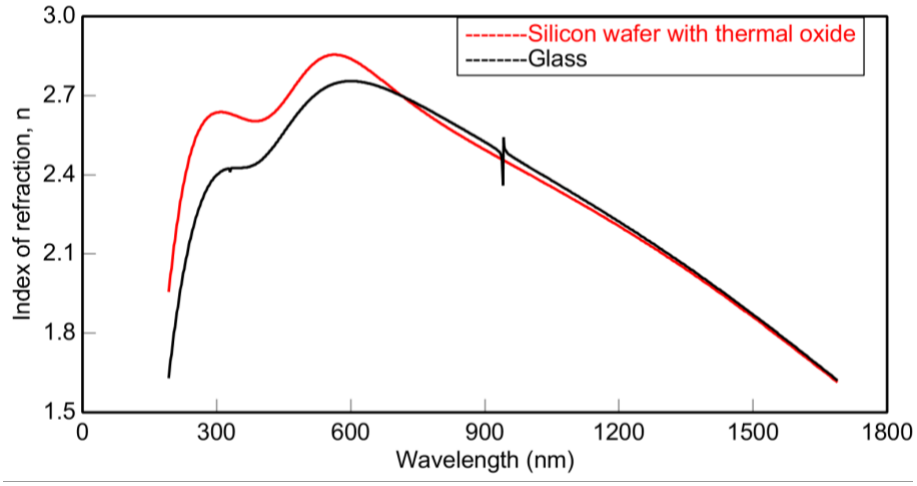

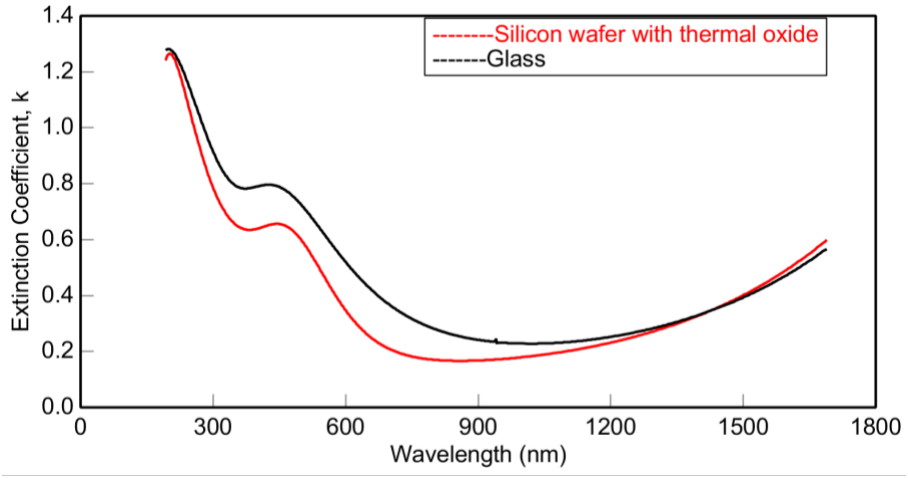

Fig. 5.14 The index of refraction, n, and extinction coefficient, k, extracted by spectroscopic ellipsometry as a function of different substrates for InN thin films

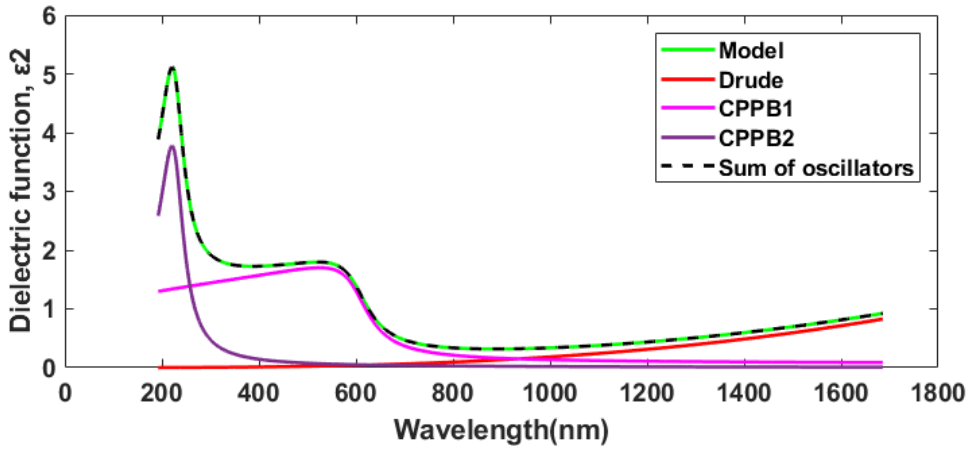

Fig 5.15 Sum of oscillators to describe optical model of InN film deposited on glass substrate.

Table 5.10 CP Energies as well as broadening of CPs for InN thin films for substrates

Substrate	**Silicon wafer with thermal oxide**		**Glass**	
	E_1	**E_2**	**E_1**	**E_2**
Broadening (eV)	0.22	0.85	0.30	1.12
CP energies (eV)	1.93	5.09	2.03	5.39

5.6 CONCLUSION

In this chapter, indium nitride thin films were deposited by reactive RF magnetron sputtering on various substrates. The effect of gas flow ratio, sputtering power, pressure and substrates were studied. It was observed that a Nitrogen gas flow ratio of at least 50%, with a power of 80W was necessary to deposit nanocrystalline films. Lowering the Pressure to 1 mTorr is resulting in c-axis oriented InN. It was also observed that films deposited on silicon wafer with thermal oxide led to films with superior electrical properties compared to glass substrates.

CHAPTER 6

SUMMARY

6.1 SUMMARY

The results of this thesis allow for a better understanding of the effect of various sputter parameters on the deposition of Aluminum Nitride and Indium Nitride thin films. Various substrates were used, including glass substrate and silicon wafer with thermal oxide (500 nm). The Aluminum nitride deposition was carried out at 200ºC and power ranging from 150 W to 200W. Indium nitride films were deposited at room temperature with power ranging from 50 W to 80 W.

The nitrogen sputtering gas percent was varied from 30% to 50% maintaining the overall gas flow rate at 20 sccm, while the pressure of the gas was varied from 1 mTorr to 5 mTorr. Characterizations of the as-deposited films included spectroscopic ellipsometry, x-ray diffraction (XRD) measurements and Hall effect measurements.

For the Aluminum Nitride thin films, it was observed that a Nitrogen gas flow ratio of at least 50%, with a power of 200W was necessary to deposit nanocrystalline films. It was also observed that films deposited on silicon wafer with thermal led to higher crystalline phase compared to glass substrates.

For the Indium Nitride thin films, it was observed that a Nitrogen gas flow ratio of at least 50%, with a power of 80W was necessary to deposit nanocrystalline films. It was also observed that films deposited on silicon wafer with thermal oxide led to superior electrical properties compared to glass substrates.

6.2 FUTURE WORK

Future work includes implementing this deposition process to deposit ternary alloy of Indium and Aluminum Nitride, producing thin films at reasonably high deposition rates and to effectively fabricate a thin film transistor device with Aluminum nitride as a gate dielectric.

REFERENCES

[1] Hopkinson, Mark. “With Silicon Pushed to Its Limits, What Will Power the next Electronics Revolution?” The Conversation, http://theconversation.com/with-silicon-pushed-to-its-limits-what-will-power-the-next-electronics-revolution-46287. Accessed 3 Apr. 2020.

[2] “III–V Integration & Devices.” III–V Material Integration, IBM Research Zurich, Accessed 15 March 2020. zurich.ibm.com/st/nanodevices/monolithicgrowth.html

[3] Pearton, S.J., “Growth and Doping of Defects in III Nitrides,” *GaN and Related Materials II,* CRC Press, 2000, pp. 113-138.

[4] Griffiths, Steven Herbert. *Bulk Group-III Nitride Crystal Growth in Supercritical Ammonia-Sodium Solutions*. 2017. University of California, PhD dissertation. ProQuest. search.proquest .com/docview/1938234151/fulltextPDF/30B33F3C00894C55PQ/1?accountid=12967.

[5] Evelyne Gil, Yamina André, Robert Cadoret, and Agnès Trassoudaine, “2 - Hydride Vapor Phase Epitaxy for Current III–V and Nitride Semiconductor Compound Issues.”, *Handbook of Crystal Growth (Second Edition),* edited by Thomas F. Kuech, North-Holland, 2015, pp. 51-93.

[6] D. Ehrentraut and T. Fukuda, "*The Ammonothermal Crystal Growth of Gallium Nitride—A Technique on the Up Rise*," in Proceedings of the IEEE, July 2010, vol. 98, no. 7, pp. 1316-1323. doi: 10.1109/JPROC.2009.2029878

[7] Haipeng Tang and James B. Webb, “Molecular Beam Epitaxy for III-N materials,” *III-Nitride Semiconductor Materials,* world scientific publishing co, 2006, pp.117-160.

[8] N Izyumskaya, V Avrutin, K Ding, Ü Özgür, H Morkoç and H Fujioka, “*Emergence of high quality sputtered III-nitride semiconductors and devices,”* Semiconductor science and technology, vol.34, no. 9, July 2019 pp. 1-23, IOP Science. doi.org/10.1088/1361-6641/ab3374.

[9] “X-ray Diffraction”, *Materials Engineering*, JoVE Science Education Database, Cambridge, 2020, jove.com/science-education/10446/x-ray-diffraction.

[10] “Ellipsometry Measurements”, *Ellipsometry Tutorial*, J.A. Woollam. jawoollam .com/resources/ellipsometry-tutorial/ellipsometry-measurements.

[11] H. Fujiwara, “*Spectroscopic ellipsometry: Principles and applications*”, John Wiley & Sons, 2007.

[12] Joungchel Lee and Robert W. Collins, "*Real-time characterization of film growth on transparent substrates by rotating-compensator multichannel ellipsometry*," Applied Optics, Vol. 37, Issue 19, 1998, pp. 4230-4238, OSA Publishing. doi.org /10.1364/AO.37.004230.

[13] "Hall Effect Sensor and How Magnets Make It Works", *Electromagnetism*, Electronics Tutorials, February 2018. electronics-tutorials.ws/electromagnetism/hall-effect.html

[14] leadley, david. "Hall Effect Measurements," *Course Handbook for Research Students*, Department of Physics, Warwick University, 2011, warwick.ac.uk/fac/sci/physics/current /postgraduate/regs/mpagswarwick/ex5/techniques/electronic/hall-effect/. /hall-effect/.

[15] D. Depla, S. Mahieu, and J. E. Greene, "Sputter Deposition Processes," *Handbook of Deposition Technologies for Films and Coatings*, Elsevier BV, 2010, pp. 253-296.

[16] Roth, J.R., *"Industrial Plasma Engineering: Principles*," Vol. 1, CRC Press, 1995.

[17] Peter Sigmund, "*Recollections of fifty years with sputtering*", Journal of thin solid films, vol.520, no. 19, July 2012, pp. 6031–6049, Elsevier BV. doi.org/10.1016/j.tsf.2012.06.003.

[18] Bloomfield, M. O., and Cale, T. S., "*Modeling of Ionized Magnetron Sputtering of Copper*," in Proceedings of the Material research society symposium, vol.616, 2000, pp. 147-152. doi.org/10.1557/proc-616-147.

[19] Iqbal, A., and Mohd-Yasin, F, "*Reactive Sputtering of Aluminum Nitride (002) Thin Films for Piezoelectric Applications: A Review*," Sensors, vol.18, no.6, 2018. doi.org /10.3390/s18061797

[20] Berg S., Nyberg T., and Kubart T., "Modelling of Reactive Sputtering Processes," In: Depla D., Mahieu S. (eds), *Reactive Sputter Deposition*, Springer Series in Materials Science, vol 109, 2008, pp. 131-152. doi.org/10.1007/978-3-540-76664-3_4.

[21] S Swann, "Magnetron sputtering," Physics in Technology, vol.19, no. 2, 1988, pp. 67-75, IOP Science. doi.org/ 10.1088/0305-4624/19/2/304.

[22] Randolph, Alvin. *Aluminum Nitride Films by Reactive Sputtering*. Rochester Institute of Technology, Master's thesis, 1996. citeseerx.ist.psu.edu/viewdoc/download?doi= 10.1.1.870.8692&rep=rep1&type=pdf.

[23] S. Loughin and R.H. French, "Aluminum Nitride (AlN)," *Handbook of Optical Constants of Solids*, Elsevier BV ,1997, pp. 373-401.

[24] "Optical properties," *InN- Indium Nitride*, NSM Archive, Accessed 31 March 2020, http://www.ioffe.ru/SVA/NSM/Semicond/InN/optic.html

[25] Wei-Chun Chen, and Shou-Yi Kuo, " *Study of High Quality Indium Nitride Films Grown on Si(100) Substrate by RF-MOMBE with GZO and AlN Buffer Layers*," Journal of Nanomaterials, vol. 2012, 2012, pp. 1-5. Hindawi, doi.org/10.1155/2012/853021.

[26] Kumar, V., and Roy, D.R, "*Structure, bonding, stability, electronic, thermodynamic and thermoelectric properties of six different phases of indium nitride*," Journal of Material Science, vol. 53, 2018, pp. 8302–8313. springer link, doi.org/10.1007/s10853-018-2176-9.

[27] Ashraful Ghani Bhuiyan, Akihiro Hashimoto, and Akio Yamamoto, "*Indium nitride (InN): A review on growth, characterization, and properties*," Journal of Applied Physics, vol. 94, no. 5, 2003, pp. 2779-2808. AIP Publishing, doi.org/10.1063/1.1595135.

VITA

Sushma Swaraj Atluri

231 Kaufman Hall
ECE Department
Old Dominion University
Norfolk, VA 23529

Education

2020 M.S.	Electrical & Computer Engineering	Old Dominion University, VA
2017 B.TECH.	Electrical & Electronics Engineering	JNTU Kakinada, India